APL Materials

P-block metal-based (Sn, In, Bi, Pb) electrocatalysts for selective reduction of CO_2 to formate

Cite as: APL Mater. **8**, 060901 (2020); https://doi.org/10.1063/5.0004194
Submitted: 08 February 2020 • Accepted: 11 May 2020 • Published Online: 11 June 2020

Zhenni Yang, Freddy E. Oropeza and Kelvin H. L. Zhang

P-block metal-based (Sn, In, Bi, Pb) electrocatalysts for selective reduction of CO_2 to formate

Cite as: APL Mater. 8, 060901 (2020); doi: 10.1063/5.0004194
Submitted: 8 February 2020 • Accepted: 11 May 2020 •
Published Online: 11 June 2020

Zhenni Yang,[1] Freddy E. Oropeza,[2,a)] and Kelvin H. L. Zhang[1,b)]

AFFILIATIONS

[1] State Key Laboratory of Physical Chemistry of Solid Surfaces, College of Chemistry and Chemical Engineering, Xiamen University, Xiamen 361005, People's Republic of China
[2] IMDEA Energy Institute, Avda. Ramón de la Sagra, 3, Móstoles, 28935 Madrid, Spain

Note: This paper is part of the Special Issue on Solar to Fuel.
[a)] **Email:** freddyoropeza@gmail.com
[b)] **Author to whom correspondence should be addressed:** Kelvinzhang@xmu.edu.cn

ABSTRACT

Electrochemical reduction of CO_2 to fuels and chemical feedstocks using renewable electricity provides a promising approach toward artificial carbon recycling to address the global challenges in energy and sustainability. The most crucial step for this technique is to develop efficient electrocatalysts capable of reducing CO_2 to valuable hydrocarbon products at a low overpotential with high selectivity and stability. In this article, we present a review on the recent developments and understanding of p-block post-transition metal (e.g., Sn, In, Pb, and Bi) based electrocatalysts for electrochemical CO_2 reduction. This group of electrocatalysts shows particularly high selectivity for reduction of CO_2 to formate or formic acid. Our main focus will be on the fundamental understanding of surface chemistry, active sites, reaction mechanism, and structure–activity relationships. Strategies to enhance the activity including morphology control, nanostructuring, defect engineering, doping, and alloying to modulate the electronic structure will also be briefly discussed. Finally, we summarize the existing challenges and present perspectives for the future development of this exciting field.

I. INTRODUCTION

A. CO_2 reduction background

Since the industrial revolution in the nineteenth century, fossil fuels such as coal, petroleum, and natural gas have been exploited as the main energy source to sustain our economy and society. Extensive consumption of fossil fuels has caused an increase in the concentration of CO_2 in the atmosphere from 278 ppm at the beginning of the industrial revolution to 410 ppm today, which has brought about environmental problems associated with the greenhouse effect of CO_2.[1,2] To alleviate these negative effects and close carbon recycle, conversion of CO_2 into value-added chemicals and fuels is proposed as a promising strategy because this process not only mitigates CO_2 emissions into the Earth's atmosphere but also produces commodity chemicals that can be used either as fuels or as precursors in many industrial chemical processes.[3–5] A variety of routes for chemical conversion of CO_2 have been explored, including thermocatalytic reduction,[6–8] photocatalytic reduction,[9–14] electrochemical reduction,[15–18] and photoelectrochemical reduction[19–22]. Among these strategies, electrochemical reduction of CO_2 to form C_1 feedstocks (such as CO) and useful fuels (e.g., formate, methanol, and ethylene) driven by electricity from renewable energy sources, such as solar and wind, has been widely proposed as a very promising sustainable solution. This is largely because the cost of renewable energy sources is projected to decrease as the conversion technologies improve. For example, the cost of solar power has plunged from 3 USD W^{-1} in 2008 to 0.5 USD W^{-1} in 2020 and is projected to further reduce below 0.05 USD W^{-1} by 2030.[2] A major milestone for the development of electrochemical CO_2 reduction technologies will be the reproducible preparation of efficient and robust

electrocatalysts to accelerate the sluggish dynamic processes of the electrochemical CO_2 reduction. High selectivity toward specific products is also a very important factor due to the high cost for product separation.

Recently, p-block metal-based catalysts, including Sn,[23–26] In[27–30], Bi,[31–33] and Pb,[34,35] have been shown to drive the electrochemical CO_2 reduction with high selectivity toward C_1 products, in particular, formate or formic acid with a selectivity of up ~100%. Metal-free carbon-based catalysts such as N-doped carbon nanotubes and N-doped fullerenes have also been shown to drive the CO_2 reduction preferentially toward formate.[36–38] Although the reported selectivities are generally lower than those of p-block metal-based catalysts, robustness and environmental friendliness are the desirable properties of these nonmetal catalysts. These are materials of interest because formate (formic acid) is a highly valued product for many industrial processes. Among the common organic acids, formic acid is the most corrosive because of its low pK_a, ~3.75, being about 10 times more ionized or acidic than acetic acid. Besides having acidic properties, formic acid behaves as an aldehyde and, hence, has reducing properties. Furthermore, formic acid can also be used as the chemical fuel for fuel cells. This has triggered great efforts to understand the underlying reaction mechanism and the structure–activity relationship that may provide rational guidelines for further improving the activity, selectivity, and stability of these types of electrocatalysts.

In this article, we will review recent developments and understanding of p-block metal-based (e.g., Sn, In, Pb, and Bi) electrocatalysts for the electrochemical CO_2 reduction reaction (CO_2RR). Although there are already a few comprehensive reviews on the electrocatalysts for the electrochemical CO_2RR,[16,17,39–43] our main focus will be specifically on the p-block metal-based electrocatalysts with high selectivity for formate production. In the following, we will start with a brief introduction to the fundamentals and challenges of CO_2 reduction, followed by classification of electrocatalysts and possible reaction pathways. We then review in detail Sn, In, Bi, and Pb based electrocatalysts, in terms of the fundamental understanding of the surface chemistry, active sites, reaction mechanism, and structure–activity relationships for the CO_2RR. Strategies to enhance the activity including nanostructures, defect engineering, doping, and alloying will also be briefly discussed. Finally, we summarize the existing challenges and present perspectives for the future development of this exciting field.

B. Fundamentals and challenges

A basic electrochemical CO_2 reduction system is composed of an anode, a cathode, an electrolyte containing dissolved CO_2, and a proton exchange membrane, as shown in Fig. 1. The cathode supplies catalytic active sites for the electrochemical CO_2RR, and the anode promotes oxidation reactions, e.g., oxygen evolution reaction (OER). The membrane separates oxidation products from reduction products while allowing the exchange of protons (H^+) to keep charge balance. The electrolyte serves as a medium to transfer charged species (e^-/H^+) and also as a medium to dissolve CO_2. Obviously, the CO_2RR at the electrocatalyst is the most crucial process for the overall electrochemical CO_2 reduction system. It is generally believed that the overall electrochemical CO_2RR process includes CO_2 solvation from the gas phase, adsorption, and

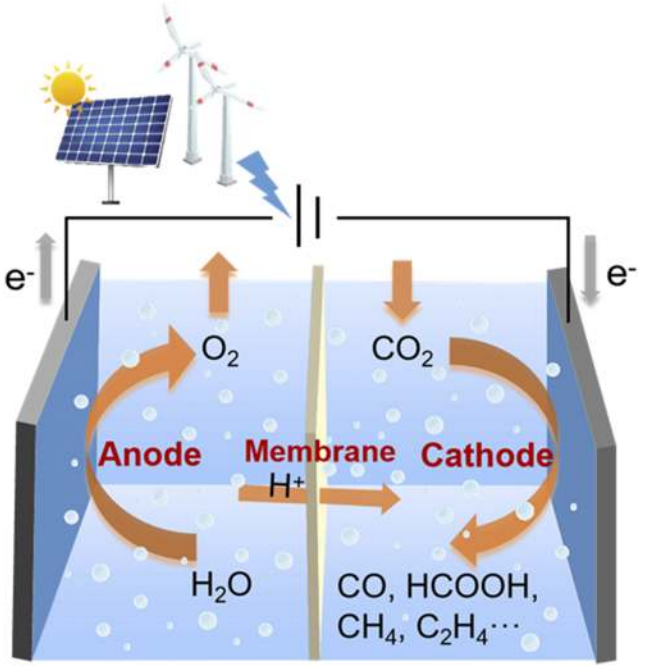

FIG. 1. Schematics of the electrochemical CO_2 reduction system. Adapted with permission from Wu *et al.*, Adv. Sci. **4**, 1700194 (2017). Copyright 2017 Wiley-VCH.

activation of CO_2 molecules on the electrocatalyst surface, followed by multiple-step proton–electron coupled transfer reactions to form hydrocarbons and desorption. Because of the complex chemical and physical processes, the efficiency and selectivity of the electrochemical CO_2RR confront many fundamental challenges, which can be grouped into the following three aspects:

(i) **Low CO_2 solubility**. The solubility of CO_2 in aqueous electrolytes is only 34 mM under the standard condition.[44] This

TABLE I. Thermodynamic equilibrium potentials (vs RHE, pH 7) of electrochemical CO_2RR in aqueous solution.[274]

No.	Thermodynamic equilibrium half-reactions	Potentials/V vs RHE
1	$CO_2 + e^- \rightarrow CO_2^{\bullet -}$	−1.49
2	$CO_2 + 2H^+ + 2e^- \rightarrow CO + H_2O$	−0.11
3	$CO_2 + 2H^+ + 2e^- \rightarrow HCOOH$	−0.20
4	$CO_2 + 4H^+ + 4e^- \rightarrow HCHO + H_2O$	−0.10
5	$CO_2 + 6H^+ + 6e^- \rightarrow CH_3OH + H_2O$	0.03
6	$CO_2 + 4H_2O + 6e^- \rightarrow CH_3CH_2OH$	−0.77
7	$CO_2 + 8H^+ + 8e^- \rightarrow CH_4 + H_2O$	0.17
8	$2CO_2 + 14H^+ + 8e^- \rightarrow C_2H_6 + 4H_2O$	0.14
9	$2CO_2 + 12H^+ + 12e^- \rightarrow C_2H_4 + 4H_2O$	0.07
10	$2H^+ + 2e^- \rightarrow H_2$	0

TABLE II. The performance of various p-block metal-based electrocatalysts for electrochemical CO_2 reduction.

Electrocatalyst	Electrolyte	Main carbon product	FE_{max} (%)	$j_{main\ product}$ at FE_{max} (mA cm^{-2})	Potential (V)	References
Sn	0.1M $KHCO_3$	Formate	88.4	5	−1.48 vs NHE	61
Sn dendrite electrode	0.1M $KHCO_3$	Formate	71.6	17.1	−1.36 vs RHE	133
Nano-SnO_2/carbon black	0.1M $NaHCO_3$	Formate	86.2	6.2	−1.8 vs SCE	157
Nano-SnO_2/graphene	0.1M $NaHCO_3$	Formate	93.6	9.5	−1.8 vs SCE	157
Sn(S)/Au	0.1M $KHCO_3$	Formate	93.3	55	−0.75 vs RHE	154
Sn nanoparticles/Au	0.1M $KHCO_3$	Formate	30.2	42	−0.75 vs RHE	154
Sn/SnO_x thin film	0.5M $NaHCO_3$	Formate CO	40 55	0.7 1	−0.7 vs RHE	141
Wire-in-tube SnO_2	0.1M $KHCO_3$	Formate	63	3.8	−0.99 vs RHE	166
Ultra-small SnO_2 NPs (<5 nm)	1M $KHCO_3$	Formate	64	92.8	−1.21 vs RHE	275
Ultra-small SnO NPs/C (2.6 nm)	0.5M $KHCO_3$	Formate	67.7	20.1	−0.86 vs RHE	158
SnO_2 porous NWs	0.1M $NaHCO_3$	Formate	80	4.8	−0.8 vs RHE	165
Sn quantum sheets/GO	0.1M $NaHCO_3$	Formate	89	21.1	−1.8 vs SCE	162
Chain-like mesoporous SnO_2	0.1M $KHCO_3$	Formate	95	10.2	−0.97 vs RHE	276
Mesoporous SnO_2 nanosheets	0.5M $NaHCO_3$	Formate	83	14	−0.9 vs RHE	277
Bi−SnO/Cu foam	0.1M $KHCO_3$	Formate	93	12	−1.7 vs Ag/AgCl	168
Reduced porous SnO_2 nanosheets	0.5M $NaHCO_3$	Formate	92.4	/	−0.7 vs RHE	169
Sn gas diffusion electrode	0.1M $KHCO_3$	Formate	64	3	−1.2 vs RHE	149
SnS_2/rGO	0.5M $NaHCO_3$	Formate	84.5	11.7	−1.4 vs Ag/AgCl	155
$Ag_{76}Sn_{24}$	0.5M $NaHCO_3$	Formate	80	19.7	−0.8 vs RHE	170
$CuSn_3$	0.1M $KHCO_3$	Formate	95	31	−0.5 vs RHE	198
GDE-$In_{0.90}Sn_{0.10}$	0.1M $KHCO_3$	Formate	92	15	−1.2 vs RHE	201
Nanoporous In−Sn	0.1M $KHCO_3$	Formate	78.6	9.6	−1.2 vs RHE	202
In	0.1M $KHCO_3$	Formate	94.9	5	−1.55 vs NHE	61
Anodized In	0.5M K_2SO_4	Formate	87.2	/	−1.7 vs SCE	30
In^0–In_2O_3 composite	0.1M Na_2SO_2	Formate	100	/	−1.8 vs Ag/AgCl	278
Hierarchical porous In	0.1M $KHCO_3$	Formate	90	60.8	−1.2 vs RHE	205
Dendritic In foams	0.5M $KHCO_3$	Formate	86	5	−0.86 vs RHE	27
In_2O_3−rGO	0.1M $KHCO_3$	Formate	84.6	/	−1.2 vs RHE	225
H−InO_x nanoribbons	0.5M $NaHCO_3$	Formate	91.7	5	−0.7 vs RHE	279
Sulfur-doped indium	0.5M $KHCO_3$	Formate	93	58.9	−0.98 vs RHE	210
$Cu_{25}In_{75}$	0.5M $NaHCO_3$	Formate	84.1	5.3	−0.7 vs RHE	214
$Cu_{94}In_6$	0.5M $NaHCO_3$	CO	88.1	4	−0.6 vs RHE	214
In/Cu	0.1M $KHCO_3$	CO	90.4	5.8	−0.8 vs RHE	280
CuIn alloy nanowires	0.5M $KHCO_3$	CO	68.2	3.9	−0.6 vs RHE	281
Cu−In	0.1M $KHCO_3$	CO	95	/	−0.7 vs RHE	218
Ultrathin Bi nanosheets	0.5M $NaHCO_3$	Formate	90	11	−1.5 vs SCE	251
Defect rich Bi	0.5M $NaHCO_3$	Formate	84	5	−0.75 vs RHE	282
Nanotube-derived Bi	0.5M $KHCO_3$	Formate	~100	60	−1.05 vs RHE	254
Bi NPs/Bi_2O_3 NSs	0.5M $KHCO_3$	Formate	~100	24.4	−1.16 vs RHE	256
2D mesoporous Bi nanosheets	0.5M $NaHCO_3$	Formate	~100	18	−1.1 vs RHE	33
Bi nanoflowers	0.5M $KHCO_3$	Formate	99.2	7.5	−1.5 V vs SCE	283
Bi nanoflakes	0.1M $KHCO_3$	Formate	~100	1	−0.6 vs RHE	284
P-orbital localized-Bi	0.5M $NaHCO_3$	Formate	95	54.1	−1.16 vs RHE	285
Bi_2O_3−NGQDs	0.5M $KHCO_3$	Formate	98	16.6	−0.87 vs RHE	259
Bi_2O_3–CuO(0.75)	0.5M $KHCO_3$	Formate	89.3	9.1	−1.4 vs SCE	286
Oxide-derived Bi−Sn/CF	0.5M $KHCO_3$	Formate	96	63	−1.14 vs RHE	203
Pb	0.1M $KHCO_3$	Formate	97.4	5	−1.63 vs NHE	61
0.78 Ml Pb/Cu	0.1M $KHCO_3$	Formate	74.2	/	−1.14 vs RHE	268
$Sn_{56.3}Pb_{43.7}$	0.5M $KHCO_3$	Formate	79.8	45.7	−2.0 vs Ag/AgCl	204
Sulfide-derived (SD)-Pb	0.1M $KHCO_3$	Formate	88	12	−1.08 vs RHE	266

low solubility limits the CO_2 mass transport rate and the reduction rate on the electrocatalysts and, therefore, limits the current densities to a few tens of mA cm^{-2}. In order to reach an industrially viable CO_2 reduction rate, some cell design schemes that increase the solubility and mass transport to the electrodes have been recently proposed, such as flow cells or gas diffusion electrodes.[45–49] Furthermore, ionic liquid and organic electrolytes are also developed to increase the CO_2 solubility and reaction kinetics.[50–53]

(ii) **Large overpotential**. The thermodynamic cost of reducing CO_2 is comparable to that for the hydrogen evolution reaction (HER). For example, thermodynamic equilibrium potentials [versus reversible hydrogen electrode (RHE)] for the reduction of CO_2 to CO and formic acid are −0.11 V and −0.20 V, respectively.[54] However, a large activation energy barrier is required to activate CO_2 molecules, which results in large overpotential requirements to drive the overall reaction. Therefore, a key factor to drive the CO_2RR at lower overpotentials lies at the activation of CO_2 molecules, which is fundamentally difficult because of the inherent chemical stability of CO_2 associated with a linear centrosymmetric molecular structure and large bonding energy of C=O double bond (~750 kJ mol^{-1}).[55] Furthermore, the CO_2 reduction process may involve complicated proton-coupled multistep electron transfer reactions that result in the sluggish reaction kinetics. As a result, a high reduction potential of −1.49 V vs RHE is required to form the key intermediate CO_2^- radicals through the initial one-electron transfer process, making the reaction energetically prohibitive to take place.[56,57]

(iii) **Poor selectivity**. The large overpotentials required to activate CO_2 lead to the formation of highly reactive species, i.e., bent CO_2^- radicals. Slight potential differences result in divergent reaction pathways via 2, 4, 6, 8, 12, or even more electron transfer and produce a large spectrum of products, including CO, formate, methane, methanol, and ethylene (see Table I).[58,59] Furthermore, due to the large cathodic potential required to drive the CO_2 reduction, the HER becomes a competitive side reaction in aqueous solutions, which detrimentally further impacts the selectivity for CO_2 reduction.[60] The separation of complicated products would impose additional costs for electrochemical CO_2RR technologies. Hence, developing electrodes with high selectivity to a specific product is highly desirable in this field (Table II).

II. ELECTROCATALYSTS AND REACTION MECHANISMS

Since the pioneering works by Hori *et al.* in the 1980s and 1990s,[61–63] great efforts have been devoted to the development and understanding of electrocatalysts for electrochemical CO_2 reduction, especially within the past decade.[17,43,64–67] According to the major products of CO_2 reduction (i.e., the selectivity), electrocatalysts can be classified into four groups, as graphically shown in Fig. 2, including *group I*, transition metals, such as Fe, Ni, Pd, and Pt, which catalyze mostly the HER; *group II*, metals, such as Ag, Au, and Zn whose major product is CO; *group III*, Cu and its derived oxides,

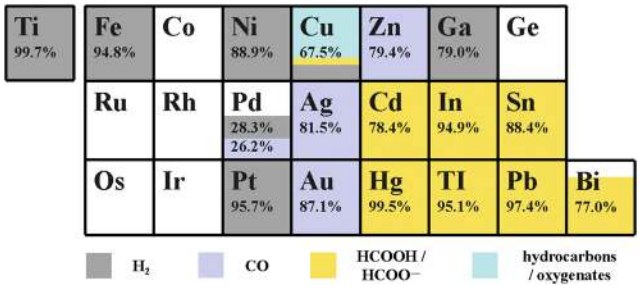

FIG. 2. Partial Periodic Table depicting primary products of metal catalysts for CO_2 electroreduction (based on experimental data from Hori[61]). Four groups include metals for H_2 (gray), formic acid (yellow), CO (purple), and hydrocarbons/oxygenates (blue).

which promote the formation of hydrocarbons or oxygenates; and *group IV*, p-block metals (Sn, In, Bi, and Pb) and their oxides, primarily producing formate or formic acid.[61]

Over the past few decades, the reaction pathways on different electrocatalysts have been studied both experimentally and theoretically.[17,64,68,69] It is generally agreed that the rate-determining step (RDS) of CO_2RR is the first electron transfer to surface-adsorbed $^*CO_2$ (where * denotes the adsorption site) to form $^*CO_2^{\bullet-}$ radicals [Fig. 3(a)]. The next protonation step is determined by which atom binds to the electrode surface. If the carbon atom of $^*CO_2^{\bullet-}$ binds strongly to the surface, the oxygen atom would be protonated to form *COOH, while if the oxygen atoms bind to the surface, the carbon atom would be protonated to form *OCHO. The selectivity and activity toward the CO_2RR of the above-mentioned groups are essentially determined by the relative binding strength of the reaction intermediates (*OCHO, *COOH, *CO, and *H) on the surfaces.[70,71] For instance, a very strong interaction between *CO and late transition metals such as Pt and Ni in *group I* prevents the adsorbed *CO to desorb as CO or its further reduction, leading to H_2 as the main product. On the other hand, more balanced interaction between CO_2 reduction intermediates and catalysts in *groups II* to *IV* leads to the formation of various CO_2 reduction products. In the case of *group II*, including Au, Ag, and Zn, a relatively weak binding strength of *CO with the catalyst surface benefits the desorbed *CO and formed CO. Cu and Cu oxides bind *CO with the moderate strength so that further reduction and reactions (e.g., C—C coupling) may occur to form a wider product distribution, such as methane, methanol, ethylene, and other multicarbon products, via *CHO/*COH intermediates. Finally, post-transition metals in *group IV* possess a particularly high selectivity toward CO_2 reduction against the HER because *H binds weakly to these metal surfaces, therefore inhibiting the HER. Additionally, the characteristic oxophilicity of p-block metals favors the formation of oxygen-bond intermediates such as *OCHO (over carbon-bond *COOH), which have been shown to be key intermediates for the production of formate or formic acid as the major product [Fig. 3(a)].

To summarize, the binding strength of key intermediates on the metal electrode surfaces not only explains the selectivity trends observed in different groups but also guides the possible

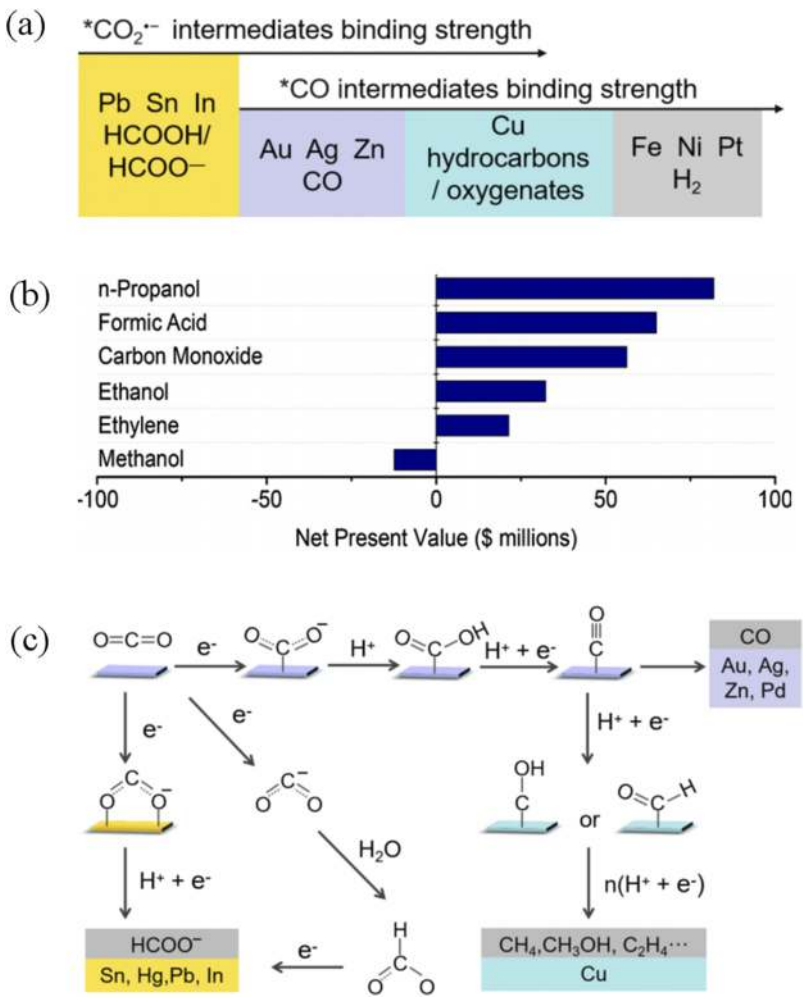

FIG. 3. (a) The relationship between CO_2RR intermediates' binding strength and product composition. (b) The end-of-life net present value (NPV) from a generalized CO_2 electrolyzer system for the production of 100 tons per day of various CO_2 reduction products. Reprinted with permission from Jouny *et al.*, Ind. Eng. Chem. Res. **57**, 2165–2177 (2018). Copyright 2018 American Chemical Society. (c) Reaction mechanism of electrochemical CO_2 reduction on different metals in aqueous solution.

reaction mechanisms proposed for product formation. It provides guidance for rationally designing electrocatalysts for CO_2 reduction. In the following, we will briefly discuss the different electrochemical CO_2RR behaviors on *group II*, *III*, and *IV* electrocatalysts.

A. Electrocatalysts for CO production (Ag, Au, and Zn)

Group II metals, Au,[72–76] Ag,[77–81] and Zn,[82–85] show the highest selectivity for CO production. CO is an important feedstock for the water–gas shift reaction and Fischer–Tropsch synthesis.[86–89] To form CO, the reaction pathway begins with chemical adsorption of CO_2 on the catalyst surface, followed by the formation of the COOH* intermediate [shown in Fig. 3(c)]. The adsorbed COOH* intermediate is further reduced by the reaction with another proton and electron, yielding CO and H_2O. Based on this reaction pathway, suitable catalysts for CO production should have a strong binding to COOH* and a weak binding to *CO. However, according to the density functional theory (DFT) calculations by Nørskov, the adsorption energies of *CO and *COOH on these metal surfaces usually vary parallelly; it is hard to induce an increase in the binding strength of *COOH to the surface without increasing the *CO adsorption energy at the same time.[64]

Many attempts have been done to optimize the activity/selectivity of Au, Ag, and Zn for CO. Surface morphology,[90,91] catalyst size,[92,93] and structure[94,95] play important roles in the activity and faradaic efficiency (FE) toward the reduction of CO_2 to CO because these factors determine the type and number of surface sites exposed as active sites. For example, nanostructured Ag can improve FE of CO up to 92%.[96] The intrinsic activity of nanostructured Ag has also been shown to increase by 20 times as compared with polycrystalline bulk metals under an overpotential of 0.5 V, which is attributed to the highly curved nanostructure surface because it can stabilize CO_2^- intermediates and decrease the activation barrier. Furthermore, electronic effects, modulated by alloying,[97,98] doping,[99] and forming defects,[54,85] and reaction conditions, such as temperature,[100,101] pressure,[102] and electrolytes,[77,103,104] also have a significant influence on electrochemical CO_2RR performances.

B. Cu and oxide-derived electrocatalysts

Cu and its derivative compounds are unique catalysts that can directly convert CO_2 into a wide variety of hydrocarbon and oxygenate products (CH_4, CH_3OH, C_2, and C_{2+}).[105,106] The selective conversion of CO_2 into C_2H_4 or C_{2+} is highly valuable because such products can be directly used in the existing chemical industry. However, large kinetic barriers for producing C_2H_4 or C_{2+} on Cu surfaces lead to unsatisfactory current density and uncompetitive FE at a low overpotential. Great efforts have been devoted to understanding the reaction mechanism and to modulating the structure and electronic properties of the catalysts to increase the activity and selectivity,[107,108] for instance, by nanostructuring,[109,110] alloying,[111–115] controlling crystal facets,[116–118] and grain boundaries (GBs).[119]

CH_4 and CH_3OH. $^*CO$ is likely the common intermediate for the production of CH_4, CH_3OH, and C_{2+}. For CH_3OH, the $^*CO$ intermediates need to undergo a series of hydrogenation reactions to form $^*OCH_3$ intermediates. Since protons could combine with a carbon atom instead of oxygen atoms, the next proton–electron coupled transfer process results in a competition between methanol and methane formation. Back *et al.* introduced the OH binding energy as a selectivity determining descriptor to evaluate the possibility of producing these two products.[120] The catalyst with a weak OH binding energy is selective to the methanol formation. On the other hand, a strong OH binding energy leads to C—O dissociation coupled with C—H bond formation and therefore a much higher selectivity toward CH_4.

C_2 and C_{2+} products. The sufficient coverage of various intermediates such as $^*CO$, $^*CH_2$, and $^*CH_3$ and the C—C coupling reaction is the necessary condition to obtain C_2 and C_{2+} products.[121] Provided that the kinetic barrier of C—C bond formation is much larger than that of C—H and C—O, the formation of C_2 products such as acetaldehyde, ethylene, and ethanol requires larger overpotentials and usually these products are obtained with a lower FE in comparison to that of simple C_1 products. It is difficult to identify the formation mechanism of multicarbon products, because of the multi-step proton–electron coupled transfer occurring during the process. As a result, there is an open debate on whether C_2H_6 is formed by the dimerization of $^*CH_3$ species or results from further hydrogenation of C_2H_4/$^*OCH_2CH_3$ related intermediates.[122]

C. P-block metal-based electrocatalysts

P-block metals such as Sn, In, Bi, Pb, and their oxides catalyze CO_2 reduction to formate or formic acid as major products with FE greater than 90% in CO_2-saturated aqueous solution.[61] Compared with others, formate is a highly desirable and profitable product shown in Fig. 3(b).[123] It is one of the attractive candidates as a liquid fuel for the hydrogen economy because of its high energy density, and it is considered as an important raw material for the production of various organic agents.[124,125] Compared to CH_3OH and CH_4 with six- and eight-electron reactions, respectively, the two-electron transfer route for formate formation has more opportunity to achieve the high FE, and it seems more commercially viable at the present stage.[126–128]

The reaction pathways for these types of electrocatalysts are shown in Fig. 3(c). There are two pathways to form formate or formic acid ($HCOOH/HCOO^-$): (i) via direct carbon-bond $^*COOH$ intermediates from stabilized $^*CO_2^{\bullet-}$ radicals, as described by Hori *et al.*,[61] and (ii) through a proton–electron coupled transfer process via $^*OHCO$ ($^*OCHO^*$ or HCO^*O^*) intermediates.[129] DFT calculation by Yoo *et al.* suggested that there is a strong linear correlation between the free energies of $COOH^*$ and H^*.[129] If the formation of HCOOH proceeds via the $COOH^*$ intermediate, it is inevitable to face with the competitive HER. Therefore, there is a growing agreement that the reaction pathway via $^*OHCO$ intermediates is more plausible for these highly selective electrocatalysts.

Formate formation on nonmetallic electrocatalysts. Although the catalytic activity of pure carbon materials toward the electrochemical reduction of CO_2 can be neglected, heteroatom-doped carbon electrocatalysts exhibit high catalytic activity because the charge distribution of the carbon materials is modified, which modulates the intermediate formation energies.[15,36] The highest formate selectivity by carbon-based materials has been achieved upon N-doping, forming pyridinic N active sites.[37,38,130] The reaction mechanisms proposed for nonmetallic electrocatalysts are more elusive than those proposed for metallic electrocatalysts, possibly due to a fewer amount of studies carried out with these types of electrocatalysts. On one hand, some experimental studies and DFT calculations propose the direct carbon-bond $^*COOH$ intermediate mechanism as plausible for the CO_2 reduction on N-doped carbon electrodes.[37,130] Although N doping does not favor the adsorption of $^*COOH$, it seems to favor the desorption of HCOOH, which is a key factor for high formate selectivity.[130] On the other hand, Wang *et al.* proposed that pyridinic N provides basicity to adjacent C, which enhances the CO_2 adsorption. Subsequently, the adsorbed CO_2 molecule is reduced to a stabilized COO^* radical instead of $^*COOH$ intermediates. A second rapid electron transfer and protonation lead to the formation of formate as the main product.[131]

III. P-BLOCK METAL-BASED ELECTROCATALYSTS

A. Tin-based electrocatalysts

Sn-based materials have been identified as attractive electrocatalysts for selectively reducing CO_2 to formate due to their good activity, high selectivity, non-toxicity, and abundance in the Earth's crust for large scale applications.[127,132,133] Numerous Sn-based electrocatalysts have been investigated in the past few years.[134–137] In 1994, Hori *et al.* first reported that metallic Sn was active for electrochemical CO_2 reduction with high formate selectivity (FE ≈ 88%) in 0.1M $KHCO_3$ aqueous solution.[61] Following Hori's seminal work, large research efforts have devoted to studying the active site and reaction mechanism of the CO_2RR on Sn-based electrocatalysts. In the following, we will provide a brief review on relevant studies of the active site and strategies for improving the catalytic performance, including (i) increasing the number of active sites by morphology control and nanostructuring and (ii) increasing the intrinsic activity by electronic modulation via doping, alloying, and defects.

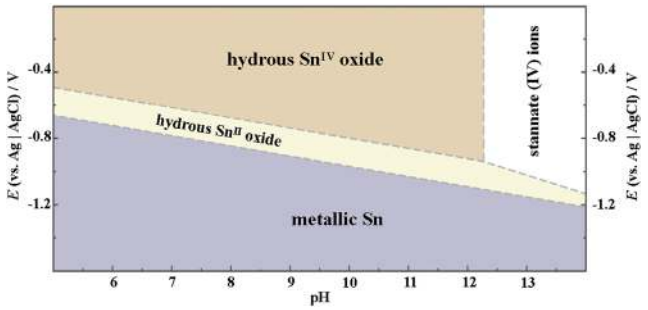

FIG. 4. The Pourbaix diagram of Sn, showing thermodynamic stability regions of various Sn oxidation states. Reprinted with permission from Dutta *et al.*, Nano. Energy **53**, 828–840 (2018). Copyright 2018 Elsevier Ltd.

1. Active sites and reaction mechanism

It is known that a pure Sn metal surface tends to be oxidized to SnO or SnO_2 when exposed to air. However, according to the Pourbaix diagram (Fig. 4), under CO_2RR conditions, the oxidized states of Sn are unlikely to exist on the Sn surface because the large cathodic potential needed for formate production is much more negative than the standard reduction potential for Sn oxides.[138] Therefore, early works generally assumed that the bare metallic Sn surface was the active site for CO_2RR (see Refs. 61, 139, and 140). The large overpotential for CO_2 was attributed to the large kinetic barrier for electron transfer from Sn to CO_2 to form the initial CO_2^- intermediate.[141] This mechanism is also commonly invoked for many other metal electrodes.[59]

However, it should be noted that the Pourbaix diagram is based on thermodynamics considerations and ignore kinetics.[142] Even though the potential for the CO_2RR past the reduction potentials for metal oxides, metastable metal oxides were known to persist on electrode surfaces during cathodic reactions.[143–146] In addition, the reported CO_2RR activities of Sn electrodes are strongly dependent on the pretreatment conditions for the Sn electrodes used in different studies.[133,139,147] Based on these considerations, Chen and Kanan carefully compared the CO_2RR activities of Sn electrodes subjected to different pretreatments and demonstrated that SnO_x is essential for the CO_2RR.[141] In particular, they showed that a Sn electrode with a native SnO_x layer exhibited a potential-dependent CO_2 reduction activity consistent with previously reported activity by Hori *et al.* On the other hand, etching off the SnO_x layer from the electrode leads to negligible activity for the CO_2RR and higher HER selectivity. However, an electrode deliberately prepared with a mixed phase of Sn and SnO_x resulted in much higher CO_2RR activity than that of the pristine Sn foil, showing an eightfold increase in the current density and fourfold increase in formate FE (Fig. 5). Although it was not clear whether the CO_2RR occurs on the SnO_x surface or at the interfaces between Sn^0 and SnO_x, the authors proposed that the presence of SnO_x may provide a facile pathway for electron transfer to the stabilized CO_2^- intermediate.[141,148,149] Nevertheless, insights from this seminal work provide an important guideline to prepare metal/metal oxide composite electrocatalysts with superior activity. Bocarsly and co-workers used *in situ* attenuated total reflection infrared spectroscopy (ATR-IR) to study the mechanism of CO_2 reduction on Sn electrodes. Their experiments further proved that a surface SnO_x layer is stable under the reducing potential conditions for the CO_2RR and is crucial for formate formation.[148] Furthermore, their study also suggests that surface-bound Sn carbonates are crucial reaction intermediates for transforming CO_2 into formate. As shown in Fig. 6, it was proposed that the reduction of CO_2 is preceded by a two-electron reduction of the electrode from a native SnO_2 to a Sn^{II} oxyhydroxide. The Sn^{II} species then react with CO_2 to form the surface-bound Sn carbonates, as evidenced by their *in situ* ATR-IR. Tin carbonate undergoes the necessary transfers of two electrons and a proton to form formate, which quickly desorbed, and the surface returns to the Sn^{II} oxyhydroxide surface.

In operando spectroscopic methods such as x-ray absorption spectroscopy (XAS) and Raman spectroscopy have also been employed to monitor the structural changes of electrocatalysts during the reaction process.[150] As shown in Fig. 7, concentrations of the three oxidation states (Sn^{4+} in SnO_2, Sn^{2+} in SnO, and Sn^0) were found to dynamically change in a different range of potentials. A large amount of SnO starts to form at −0.8 V vs Ag/AgCl and reaches the maximum at −1.1 V vs Ag/AgCl. In the moderate potential window, SnO_x ($1 < x < 2$) with mixed oxidation states shows a maximal FE for formate production. When the potential is more negative than −1.5 V vs Ag/AgCl, the SnO_2 nanoparticles are basically reduced to Sn^0, and at the same time, the FE for formate is significantly decreased. *In operando* Raman spectroscopy was also used to monitor the oxidation state changes of SnO_2 during the CO_2RR process. The efficiency of formate production was

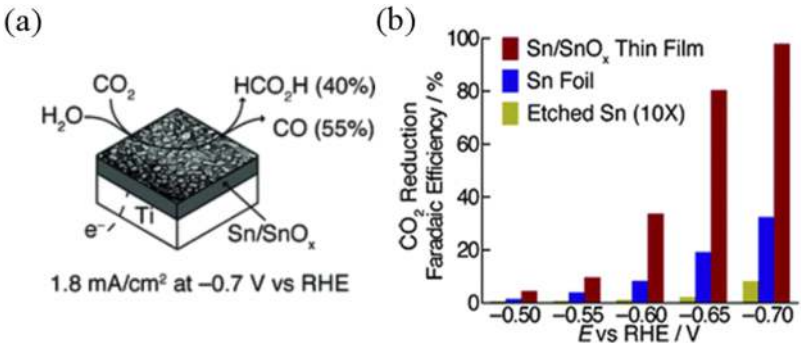

FIG. 5. (a) The illustration of mixed Sn/SnO_x thin film on the Ti electrode. (b) Comparison of the FE for formate formation on the Sn foil, etched Sn, and Sn/SnO_x mixed phase electrodes at different potentials vs RHE. Reprinted with permission from Chen and Kanan, J. Am. Chem. Soc. **134**, 1986–1989 (2012). Copyright 2012 American Chemical Society.

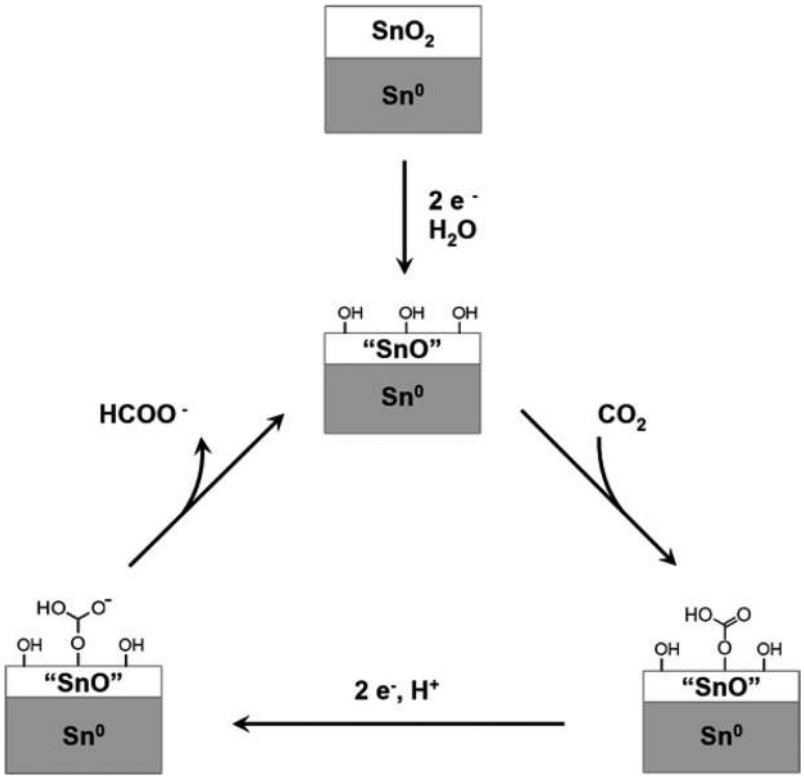

FIG. 6. Schematic diagram of the suppositional mechanism of CO_2 reduction to formate on the Sn/SnO_x electrode. "SnO" on Sn^0 refers to a Sn^{II} oxyhydroxide species. Reprinted with permission from Baruch *et al.*, ACS Catal. **5**, 3148–3156 (2015). Copyright 2015 American Chemical Society.

significantly decreased after SnO_2 was reduced to metallic Sn. Experiments and DFT calculations by Deng *et al.* also suggested that the SnO_x layer plays a pivotal role in boosting CO_2 adsorption via the formation of optimal coverage of hydroxyl groups on the electrode surface.[151] These results provided strong evidence of the importance of Sn oxides for the CO_2RR to formate.

Although the presence of a SnO_x surface layer is crucial for the electrochemical CO_2RR, its thickness should be optimized. Too thick SnO_x layer may cause a negative effect. Zhou and co-workers studied the dependence of formate selectivity on the thickness of SnO_x on Sn nanoparticles with a size of ~100 nm.[149] They found that nanoparticles with ~3.5 nm thick SnO_x exhibited the optimal formate selectivity of 64% at −1.2 V vs Ag/AgCl, and a further increase in SnO_x thickness decreased the formate selectivity but led to an increase in CO and H_2 formation.

The mechanistic studies of the CO_2RR on Sn metal or its metal oxides have been mainly based on DFT calculations.[136,152,153] The strong scaling relationship between the free energies of COOH* and H* indicates that the formation of formate with high selectivity is unlikely to involve the COOH* intermediate.[129] Instead, the free energy of *OCHO formed by the proton–electron transfer process decouples with that of H*, and therefore, it is likely the intermediate for producing HCOOH or formate.[129] Jaramillo's group combined experiments and DFT calculations for CO_2RR on a series of metal catalysts including Sn, Au, Ag, Cu, Zn, Pt, and Ni to understand the reaction mechanism and key intermediates for formate production.[147] Interestingly, a clear volcano curve (Fig. 8) is observed with Sn sitting at the top of this volcano when the binding energy of *OCHO is used as a descriptor for CO_2 reduction to formate, i.e., Sn exhibits the optimal *OCHO binding energy for the highest activity toward formate production.[147,152] However, it should be noted that the catalyst surfaces (i.e., metallic Sn) used for DFT calculations are different from the real surface (Sn/SnO_x) observed experimentally.[145] Furthermore, the highest activity of metallic Sn predicted by DFT is contradictory to the experimental results by Chen and Kanan that showed pure metallic Sn having a low CO_2RR activity. Experimental results suggest that the surface-bound Sn carbonate is the crucial reaction intermediate for transforming CO_2 into formate. Thus, DFT calculations based on the "real" surface (Sn/SnO_x) is necessary to address this discrepancy.

Interestingly, besides O, sulfur on the surface may also enhance the CO_2RR. Similar to SnO_x, SnS_x could also be electrochemically reduced to metallic Sn with residual sulfide on the surface facilitating the CO_2RR. Zheng and co-workers used atomic layer deposition of SnS_x on Au substrates, followed by an electrochemical reduction process to synthesize sulfur-modulated tin [Sn(S)] catalysts.[154] XAS studies reveal a higher oxidation state of Sn in Sn(S) compared with Sn in Sn nanoparticles. The Sn(S)/Au accelerates the CO_2RR at geometric current densities of 55 mA cm^{-2} with a FE of 93% for formate formation at −0.75 V vs RHE in 0.1M $KHCO_3$. Furthermore, Sn(S) catalysts show excellent stability for more than 40 h of operation. The authors suggested that the

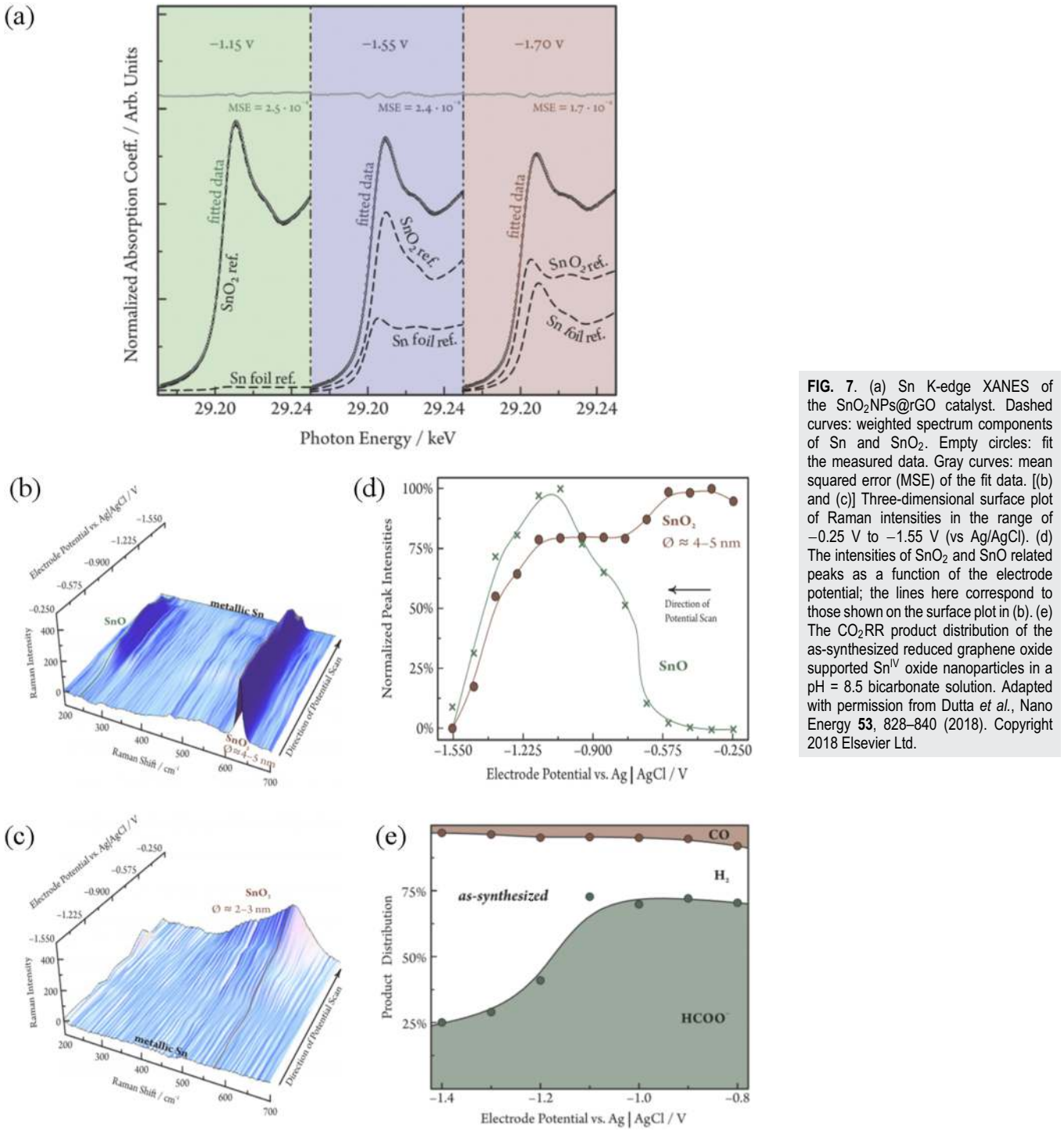

FIG. 7. (a) Sn K-edge XANES of the SnO_2NPs@rGO catalyst. Dashed curves: weighted spectrum components of Sn and SnO_2. Empty circles: fit the measured data. Gray curves: mean squared error (MSE) of the fit data. [(b) and (c)] Three-dimensional surface plot of Raman intensities in the range of −0.25 V to −1.55 V (vs Ag/AgCl). (d) The intensities of SnO_2 and SnO related peaks as a function of the electrode potential; the lines here correspond to those shown on the surface plot in (b). (e) The CO_2RR product distribution of the as-synthesized reduced graphene oxide supported Sn^{IV} oxide nanoparticles in a pH = 8.5 bicarbonate solution. Adapted with permission from Dutta *et al.*, Nano Energy **53**, 828–840 (2018). Copyright 2018 Elsevier Ltd.

presence of sulfur atoms at the surface promoted uncoordinated sites and favored the selective reduction of CO_2 to formate, as supported by DFT calculations. Li *et al.* prepared SnS_2 nanosheets supported on reduced graphene oxide (SnS_2/rGO).[155] Under working potentials, the SnS_2/rGO precatalysts partially transformed to metallic Sn forming Sn/SnS_2/rGO, which showed a maximum formate FE of 85% and a current density of ~14 mA cm^{-2} at −1.4 V vs Ag/AgCl in 0.5M $NaHCO_3$.

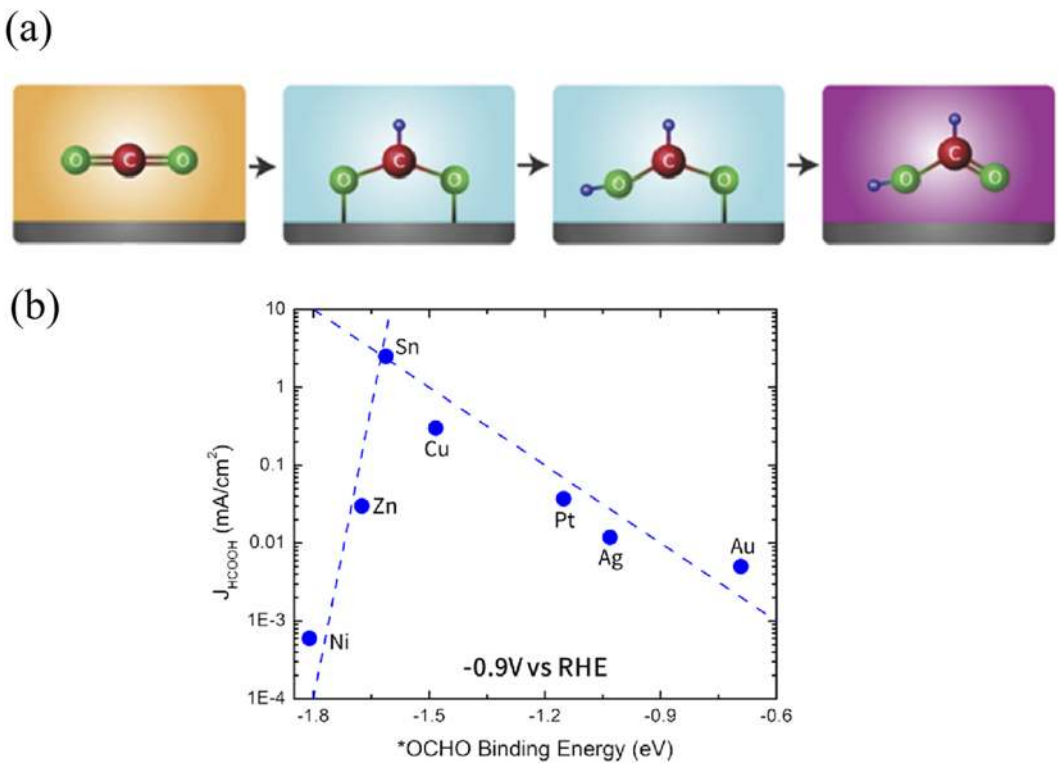

FIG. 8. (a) Mechanism pathway of electrochemical CO_2 reduction for $HCOO^-$ production via the bidentate *OCHO key intermediate. (b) Volcano curve of *OCHO binding energy and HCOOH partial current density at −0.9 V vs RHE. Reprinted with permission from Feaster *et al.*, ACS Catal. **7**, 4822–4827 (2017). Copyright 2017 American Chemical Society.

2. Morphology and nanostructure engineering

There are essentially two ways to improve the activity of Sn-based electrocatalysts: (i) morphology and nanostructure engineering to increase the number of active sites and (ii) modulating the electronic structures by doping and alloying defects or strains. Increasing the number of active sites can be achieved by controlling the particle sizes,[156–158] types of supports (e.g., carbon black, graphene, and MOF),[159–162] and nanostructure engineering (e.g., nanoparticles,[158,163,164] nanowires,[165–167] nanosheets,[155,168,169] and core–shell structure[167,170]). For example, Zhang *et al.* synthesized SnO_2 nanocrystals with sizes ranging from 3 nm to 200 nm using a hydrothermal method.[157] To maximize the specific surface area, the nanosized catalysts were loaded on high surface area carbon supports such as carbon black and graphene. It was shown that the SnO_2 nanocrystals were quickly reduced to the metallic phase at an onset potential of ~1 V [vs saturated calomel electrode (SCE)] in aqueous $NaHCO_3$ solutions. The FE for formate production exhibits a notable size dependence with 5 nm SnO_2 nanocrystals supported on graphene showing a FE over 93% and current densities >10 mA cm^{-2}[157] The authors proposed the notable reactivity toward CO_2 reduction results from a compromise between the strength of the interaction between CO_2^- and the nanoscale Sn surface and subsequent kinetic activation toward protonation and further reduction. Won *et al.* synthesized hierarchical SnO_x/Sn dendrites with a multibranched conifer-like structure and demonstrated that the formate selectivity is strongly proportional to the oxygen content in the SnO_x surface layer.[133] The unique surface morphology with a high content of oxidized Sn contributes to a large surface area and the stabilization of intermediates more effectively than the clean Sn surface. The rate of formate formation was 228.6 μmol h^{-1} cm^{-2} at −1.36 V vs RHE. Gu *et al.* synthesized ultra-small size of SnO nanoparticles supported on carbon black.[158] The ultra-small SnO nanoparticles exhibit remarkably high activity and selectivity for CO formation, which was attributed to the large surface area of the ultra-small SnO nanoparticle (numbers of active sites for activity) and the local pH effect arising from the dense packing of nanoparticles in the carbon black matrix (selectivity).

It should be noted that the change of morphology or nanostructuring not only affects the surface area but also significantly changes the numbers of surface atoms, crystal edge sites, corners sites, GBs, etc., which usually have different coordination environments compared to its bulk. This would result in different binding strengths of intermediate *COOH and *CO during the CO_2RR process. Lei and co-workers successfully synthesized ultrathin Sn 2-dimensional (2D) sheets with an averaged thickness of 1.4 nm confined in few-layered graphene.[162] The higher electrochemical active area of the ultrathin Sn sheets affords larger amounts of active sites to efficiently adsorb CO_2, as confirmed by the 9 times higher CO_2 adsorption capacity compared with that of the bulk counterpart. More interestingly, the x-ray absorption fine structure spectroscopy (XAFS) study indicates that the Sn—Sn coordination numbers in the Sn ultrathin

sheets are reduced to 1.4 and 2.7, in comparison with 2 and 4 in its bulk counterpart. The ultrathin Sn sheets display a current density of 21.1 mA cm^{-2} at −1.8 V vs SCE and a maximum FE of 89%, which is roughly 13 times larger than those of bulk Sn. Recently, single-atom catalysts (SACs) have been largely exploited due to their coordinatively unsaturated sites with unique electronic and geometric structures for the unexpected electrocatalytic performance.[171] Ni, Co, Sn, and Cu based SACs have been synthesized and exhibited high current densities and selectivity to target products.[172–177] Xie and co-workers synthesized kilogram-scale single-atom Sn dispersed on nitrogen-doped graphene using a quick freeze–vacuum drying–calcination method [Fig. 9(a)].[177] Remarkably, the $Sn^{\delta+}$ SAC exhibited a low onset overpotential (60 mV), a large turnover frequency (11 930 h^{-1}), and a long-stability (200 h) for reducing CO_2 to formate [Fig. 9(b)]. XAS and transmission electron microscopy (TEM) demonstrated that the atomically dispersed Sn atoms are positively charged ($Sn^{\delta+}$), because of the charge transfer from Sn to nitrogen-doped graphene, forming Sn—C and Sn—N bonds. The positively charged ($Sn^{\delta+}$) enables CO_2 activation and protonation to proceed spontaneously by stabilizing CO_2^{-*} and $HCOO^{-*}$, as further verified by *in situ* Fourier transform infrared spectra and DFT calculations. Furthermore, N-doping facilitates the rate-limiting formate desorption step, as verified by the decreased desorption energy from 2.16 eV to 1.01 eV and the elongated Sn—$HCOO^-$ bond length.

In addition, grain boundary (GB) engineering is also reported as an effective way to increase the CO_2 or CO electrochemical reduction.[94,119,165,166] GBs break the local symmetry and introduce disorder structure and unsaturated sites, which largely change the bonding strength of intermediates.[178] Fan and co-workers fabricated a 1-dimensional (1D) SnO_2 nanofiber with a wire-in-tube (WIT) structure, which is composed of nanoparticles interconnected through GBs.[166] The WIT SnO_2 nanofibers showed superior selectivity and stability for HCOOH production, with a FE of greater than 90%. The excellent catalytic activity was proposed to result from following aspects: (i) the large surface area of the WIT SnO_2 nanofibers, for example, is 10 times larger than that of SnO_2 nanoparticles, which may introduce more active sites for CO_2^- absorption, and (ii) the high-density of GBs could reform the bonding strengths between adsorbate and the catalyst surface to stabilize the catalytically active intermediates. Kumar *et al.* reported that SnO_2 porous nanowires with a high density of GBs exhibit a formate FE of 80% at −0.8 V vs RHE, which is 1.8 times higher than that of SnO_2 nanowires with a low density of GBs.[165] Their results suggested that GBs not only offer a larger number of active sites but also optimize the adsorption energy for intermediates.

3. Doping and alloying

Although increasing the number of active sites can improve the performance of electrocatalysts, the loading capacity and the stability of electrodes are still limitations of electrocatalytic behavior.[71] Hence, it is crucial to enhance the intrinsic activity of electrocatalysts. The intrinsic activity is determined by the binding strength of reaction intermediates with the electrocatalyst surfaces.[179,180] Therefore, tuning the surface electronic structure is the key to the development of highly efficient electrocatalysts. Strategies include doping,[181,182] alloying,[113,161,183,184] defect engineering,[185,186] and strain engineering.[187,188]

Heteroatom doping is the most common method. A series of N, Cu, S, and Bi doped Sn oxides for CO_2RR have been reported in recent years.[154,168,189–191] Doping may change the electronic properties of Sn-based materials, such as the bandgap, work function, and density of states around the Fermi level.[192,193] Tailoring these properties is an effective approach to enhance the conversion of CO_2 to HCOOH.[191,194,195] For example, An *et al.* reported that after introducing Bi atoms into SnO, the hybridization of Bi 6s and Bi 6p with the O 2p orbital leads to the formation of an additional electronic state, which helps to stabilize the $^*OCHO$ intermediate on the SnO(001) surface (see Fig. 10).[168] The Bi-doped SnO presented an excellent FE of ~93% at −1.1 V vs RHE and superior

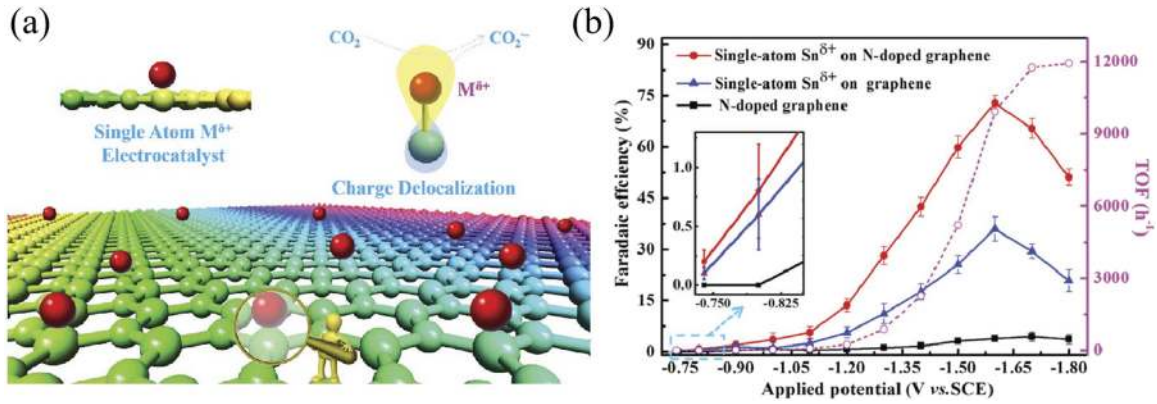

FIG. 9. (a) Schematic diagram of the single atom $M^{\delta+}$ (M stands for metals) electrocatalyst accelerating the electrochemical CO_2RR. Note that the strong metal–support interactions cause the charge density in metal atoms move toward neighboring atoms in the support, the positive charge metal atom delocalization and, hence, stabilizes the reaction intermediates such as $CO_2^{\bullet-}$, thus lowering the activation energy barriers. (b) FE toward formate and TOF of the single-atom $Sn^{\delta+}$ with/without N-doped graphene at each applied potential for 4 h, the inset gives the amplification of the selected areas of Faradaic efficiencies for formate at each applied potential for 24 h. Adapted with permission from Zu *et al.*, Adv. Mater. **31**, 1808135 (2019). Copyright 2019 Wiley-VCH.

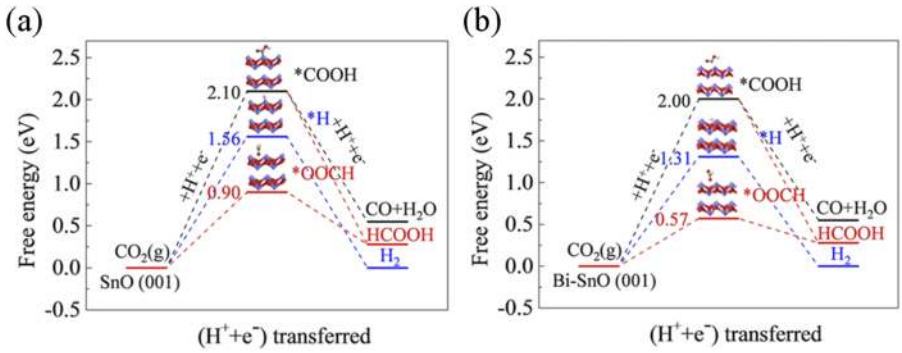

FIG. 10. Free energy diagrams of CO formation, HCOOH, and H_2 on (a) SnO(001) and (b) Bi doped SnO(001) surfaces. Reprinted with permission from An *et al.*, ACS Appl. Mater. Interfaces **11**, 42114–42122 (2019). Copyright 2019 American Chemical Society.

stability over 30 h. The authors also claimed that Bi doping can impede the reduction of Sn^{2+} during CO_2 electrochemical reduction progress.

Alloying is an attractive approach to decouple the adsorption energy of the reaction intermediates. Therefore, alloying has been shown to have a great impact on the product selectivity of CO_2RR. Many metals such as Cu,[196–198] Ag,[170,199] Au,[200] In,[201,202] Bi,[203] and Pb[204] have been alloyed with Sn to form bimetallic or ternary catalysts. Among these bimetallic catalysts, Cu−Sn has drawn much attention. Zheng *et al.* performed thermodynamic analysis of the reaction energetics using DFT calculations and found that Cu−Sn alloys could suppress the production of H_2 and CO to achieve high formate selectivity (Fig. 11).[198] They subsequently prepared Cu−Sn alloys with different Cu to Sn ratios in which they found that the $CuSn_3$ showed a formate FE of 95% at −0.5 V vs RHE and excellent stability after 50 h. A Bader analysis, *in situ* Sn L_3-edge, and Cu K-edge XAS suggest that electrons are donated from Sn to Cu, leading to a higher oxidation state of $Sn^{\delta+}$ in $CuSn_3$. This is essentially consistent with the study of single-atom $Sn^{\delta+}$ dispersion on the N-doped graphene mentioned above.[177] Bai *et al.* prepared Sn, Pd, and Pd_xSn alloys with different x values ranging from 0.25 to 4.[24] They found that the electrocatalytic activity and selectivity for HCOOH and CO were highly dependent on the surface electronic structure of the alloys. A remarkable FE of nearly 100% for HCOOH was achieved over the PdSn catalyst at the lowest overpotential of 0.26 V, while both CO formation and H_2 formation were completely suppressed. The changes in the FE for HCOOH and overpotential were in parallel with the ratio of Pd^0/Pd^{2+} in Pd_xSn, indicating that the activity for producing HCOOH is sensitive to the surface oxide species. DFT calculations suggested that the formation of the key reaction intermediate of $^*OCHO$, and the product formic acid, was the most favorable over the PdSn alloy surface.

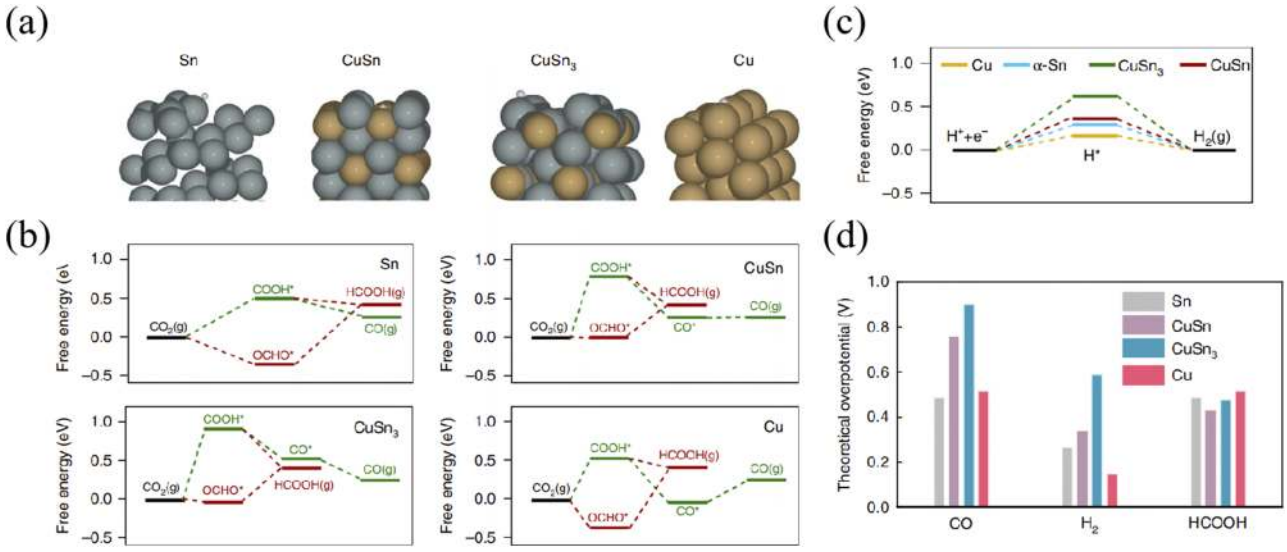

FIG. 11. (a) Optimized structures of stepped facets of Sn, CuSn, $CuSn_3$, and Cu with adsorbed H*. [(b) and (c)] Free energy diagrams for CO, HCOOH, and H_2 on Sn, CuSn, $CuSn_3$, and Cu. (d) The theoretical overpotentials for CO, H_2, and HCOOH production on stepped Sn, CuSn, $CuSn_3$, and Cu. Reprinted with permission from Zheng *et al*, Nat. Catal. **2**, 55–61 (2018). Copyright 2018 Springer Nature Singapore Pte Ltd.

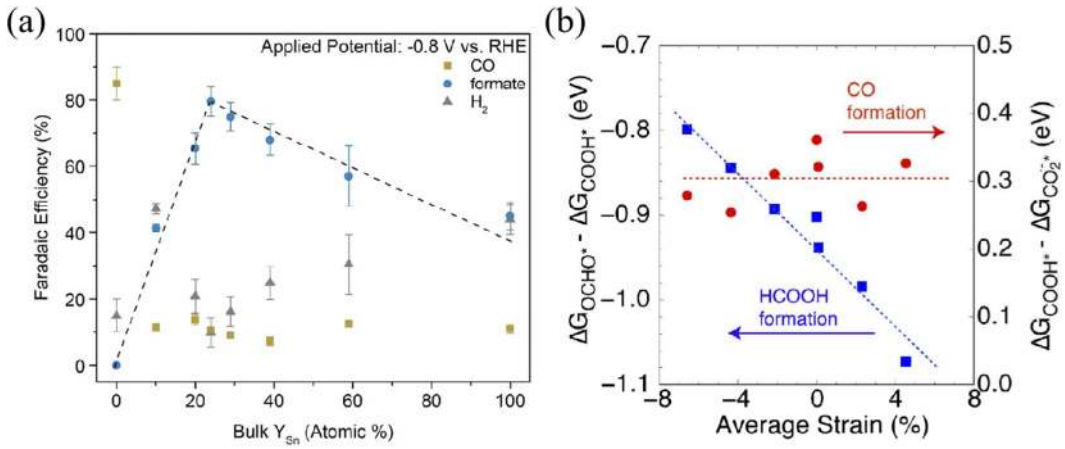

FIG. 12. (a) FE for CO, formate, and H_2 of AgSn/SnO_x catalysts as a function of the concentration of Sn. (b) The effect of the average strain on the free formation energy toward OCHO* and COOH* (left axis), and the formation of COOH* from adsorbed CO_2* (right axis). Zero represents the unstrained SnO oxygen vacancy surface. Adapted with permission from Luc *et al.*, J. Am. Chem. Soc. **139**, 1885–1893 (2017). Copyright 2017 American Chemical Society.

Luc *et al.* synthesized the Ag-doped Sn/SnO_x electrocatalyst, consisting of an Ag—Sn bimetallic core and an ultrathin shell (~1.7 nm) of partially oxidized SnO_x.[170] There is a volcano-type correlation between Sn concentration of AgSn/SnO_x catalysts and FE of CO_2 reduction to formate at −0.8 V vs RHE with a maximum FE found at 25 at. % of the Sn content [Fig. 12(a)]. The increase in Sn content in the AgSn/SnO_x alloy leads to lattice expansion [Fig. 12(b)], which stabilizes the *OCHO intermediates and facilitates the formation of formate. However, a thick SnO_x layer would form when the Sn content is over 25%, causing the decreased electrical conductivity and lower overall performance. Li and coworkers reported the tuning of Sn-based catalysts for the electrochemical CO_2RR selectively toward CO or formate by controlling the thickness of the SnO_2 layer coated on Cu nanoparticles: a thicker (1.8 nm) SnO_2 layer shows Sn-like activity to generate formate, whereas the thinner (0.8 nm) shell is selective to the formation of CO with the conversion FE reaching 93% at −0.7 V vs RHE.[23] DFT calculations suggest that the 0.8 nm SnO_2 shell-like alloys with a trace of Cu, causing the SnO_2 lattice to be uniaxially compressed and favors the production of CO over formate. The active SnO_2/Cu nanoparticle catalysts have potentials to replace the noble metal catalysts (Au and Pd) for the electrochemical CO_2RR to CO.

B. Indium-based electrocatalysts

1. Active sites and reaction mechanism

The scenario of In-based electrocatalysts for the CO_2RR is quite similar to that of Sn.[61,205–207] For example, Hori *et al.* reported that the In electrode could achieve a current density of 5 mA cm^{-2} with a FE of 94.9% for formate at −1.55 V vs SHE in 0.1M $KHCO_3$.[61] The FE of In is even higher than that of Sn (88.4%) under the same conditions. Later, comparative experiments by Bocarsly's group indicated that the FE of the In electrode toward formate largely depends on the surface conditions; an etched electrode with removal of In oxides shows low FE, while an anodized electrode with In oxides shows significantly improved a formate selectivity of >80% at −1.55 V vs SCE in CO_2-saturated 0.5M K_2SO_4.[30] Based on *in operando* ATR-IR measurements, they proposed that the formation of a redox-active In_2O_3 surface layer is essential for the high selectivity of the In electrode for formate. The In_2O_3 could react with water to form $In(OH)_3$ during the CO_2RR process, and $In(OH)_3$ can subsequently react with dissolved CO_2 to form a surface confined In—CO_3 species, which is further reduced to generate formate at a low overpotential. This reaction mechanism is consistent with the well-established CO_2 uptake by alkali hydroxides to form carbonate and water.[208] The importance of In_2O_3 in the CO_2RR was further proved by the achievement of ~100% FE for formate at −1.3 V vs Ag/AgCl on deliberately synthesized $In(OH)_3$ and In_2O_3 nanoparticles.[209]

Besides O, sulfur on the In surface may also enhance the CO_2RR performance, as recently reported by Ma *et al.*[210] In this study, S-doped In_2O_3 nanoparticles supported on carbon fibers enabled the selective CO_2RR to formate with a high FE of >85% in a broad range of current densities (25–100 mA cm^{-2}). Based on DFT calculations for the CO_2RR to HCOOH and CO on pure indium and sulfur-doped indium surfaces, the authors proposed that sulfur species could accelerate the activation of H_2O and stabilize the adsorption of the *OCHO intermediate and, therefore, give rise to the excellent selectivity and activity.

2. Morphology and nanostructure engineering

Morphology control or nanostructuring is the most straightforward method to further improve the activity of In-based electrocatalysts.[27,205,211,212] For example, Luo *et al.* prepared 3-dimensional (3D) hierarchical porous In electrodes by template-free electrodeposition on Cu meshes.[205] The porous structure provided a large surface area and exhibited a high FE for formate (~90%) in the potential range of −1.0 to −1.2 V vs RHE and reached an unprecedented formate production rate of 1.14 mmol cm^{-2} h^{-1} at −1.2 V. More interestingly, a

further electrochemical study indicated that the highly nanoporous structure of the In catalysts induced a high local pH in the vicinity of the electrode and therefore suppressed the HER and enhanced the selectivity for the CO_2RR to formate. Xia *et al.* electrodeposited dendritic In foams from Cl^--containing aqueous solution, and the dendritic In electrocatalyst exhibited an enhanced FE of 86% for formate and a current density of 5.8 mA cm^{-2} at −0.86 V vs RHE.[27] Dong *et al.* prepared an oxide-derived nanoporous In—Sn alloy with controllable morphology and size by electroreduction of indium tin oxide nanobranches.[202] When the nanopore size decreased from 1176 nm to 65 nm, the FE to formate increased from 42.4% to 78.6% at −1.1 V vs RHE.

3. Doping and alloying

Doping and alloying with other elements have also been pursued to tailor the electronic properties and hence the selectivity and activity of In-based electrocatalysts. However, different from Sn-based electrocatalysts, for most cases, In alloying with other transition metals enhanced the selectivity of CO_2RR toward CO.[213–217] In particular, Rasul and co-workers prepared the Cu—In alloy through electrochemical reduction of the thermally oxidized Cu metal foil in $InSO_4$ solution.[218] HR-TEM and EDS mapping images [Figs. 13(a) and 13(b)] suggested that In atoms preferentially locate at the surface of the Cu foil. The Cu—In electrode catalyzed the CO_2RR to CO with a FE of 90% at −0.5 V vs RHE, while the pure Cu electrode generated mixed products of CO (FE of ~45%), H_2 (FE of ~45%), and HCOOH (FE of ~10%). DFT calculations suggested that In energetically prefers to locate at the edge site of the Cu surface and modifies the local geometric and electronic structure of the Cu surface for the CO_2RR [see Figs. 13(c)–13(e)]. The presence of In weakens the adsorption of H and improves the stability of *COOH, while the *CO adsorption energy on top of the Cu atoms remains unchanged, thus explaining the suppression of the HER and COOH formation. Hoffman *et al.* prepared dendritic Cu—In alloys of various compositions and found that the products of CO_2RR depend on the alloy compositions: with an In fraction of 80 at. %, 62% FE for formate is obtained at −1.0 V vs RHE, while for 40 at. % In, formate with 49% FE and an optimal ratio of 2.6:1 (H_2:CO) syngas is produced.[216] It was suggested that the presence of two different elements at the surface, one d metal (Cu) and the other sp metal (In), may enable the modulation of the adsorption strength of *COOH and *CO intermediates and changes their trend with the applied potential, which ultimately leads to the observed product distribution.[215,218]

He and co-workers reported a particularly interesting work on the high-throughput synthesis of In_xM_{1-x} (M = Fe, Co, Ni, Cu, Zn; $0 \le x \le 1$) alloys for CO_2 reduction.[219] The selection of compositions was based on the relationship of primary products with M—CO bonding strengths [Fig. 14(a)], i.e., a high CO heat of adsorption (ΔH_{CO}) to the metal surface tends to form H_2 and hydrocarbon, while a low ΔH_{CO} value supports for HCOOH production (p-block metals).[59,220–222] The metal with a 10 kcal mol^{-1} of ΔH_{CO} is optimal for CO formation.[59] In their study, In was selected because it weakly binds with hydrogen or CO. Although In has a general character of weak binding with hydrogen or CO, alloying In with late 3d transition metals could lead to stronger M—CO bonding interactions, hence promoting CO production over the HER. This conjecture was verified experimentally for experimentally synthesized series of In_xM_{1-x} alloys [see Figs. 14(b) and 14(c)]. In appears to suppress the HER for all the alloys, and the selectivity for CO is higher than those of the pure metal electrodes. $Cu_{0.8}In_{0.2}$ shows the highest CO evolution partial current. This method indicates that the relative bond enthalpies can be used as a "descriptor" for predicting and rationally designing highly active catalysts.

Using the strong chemical interaction between electrocatalysts and supporters (e.g., reduced graphene oxide, rGO) is also a useful way to enhance conductivity and improve the activity of electrochemical CO_2RR.[223,224] Zhang *et al.* reported that the formate FE and specific current density of In_2O_3–rGO hybrid catalysts are 1.4-fold and 3.6-fold higher than those of the physical mixture In_2O_3/rGO at −1.2 V vs RHE (Fig. 15).[225] DFT calculations were further performed to simulate the change of the electronic structure and adsorption ability of intermediates. The results demonstrated that the strong chemical coupling interaction between In_2O_3 and rGO leads to faster electron transfers from rGO to In_2O_3 and a higher degree of electron delocalization in In_2O_3–rGO. The electron-rich structure has a low energy barrier to activate CO_2 and hence stabilizes $HCOO^{-*}$ and promotes the formation of formate.

Besides the electrochemical CO_2RR, In-based catalysts have been extensively explored as thermocatalysts for the hydrogenation of CO_2 to synthesize methanol and C_{5+} liquid fuels with a selectivity of 78.6%,[217,226–228] as well as photocatalysts for CO_2 photoreduction.[28,229–232] Interestingly, similar to the electrocatalysis, the presence of oxide species is important for a high catalytic activity of these systems. Finally, it should be noted that one disadvantage of In-based electrocatalysts is that the price of In metal is much higher (~10 times) than that of Sn because In is largely used as the key material for transparent electrodes in the flat panel display.[233,234]

C. Bismuth-based electrocatalysts

1. Active sites and reaction mechanism

The first report of Bi-based CO_2 reduction electrodes was presented by Komatsu *et al.* in 1995.[235] They reported 100% formate FE and current densities about 10 mA cm^{-2} in the potential region of −1.4 V to −1.7 V (vs SCE) in CO_2-saturated $KHCO_3$ solutions. However, Bi-based electrocatalysts did not receive as much attention as Sn. Research on Bi-based electrocatalysts was revisited in 2013 by Rosenthal *et al.*, whose work was concerned with CO_2 reduction in ionic liquids, in which CO was the major reduction product.[53,236] More recently, Bi-based electrocatalysts have been shown to electrochemically reduce CO_2 to formate with overall performance comparable to Sn- and In-based materials.[237–241] Bi-based catalysts prepared via electrodeposition on carbon paper have achieved a current density of 15.2 mA cm^{-2} with a formate FE of 96.4% at −1.8 V (vs SCE) in 0.5M $NaHCO_3$ saturated with CO_2.[239] In addition, Liu *et al.* recently reported Bi-based electrocatalysts prepared by growing Bi_2O_3 nanosheets on a conductive multiple channel carbon matrix using hydrothermal synthesis whose current density and formate FE were shown to reach about 17 mA cm^{-2} and 93.8% at −1.23 V vs RHE in 0.1M $KHCO_3$ electrolyte saturated with CO_2.[238]

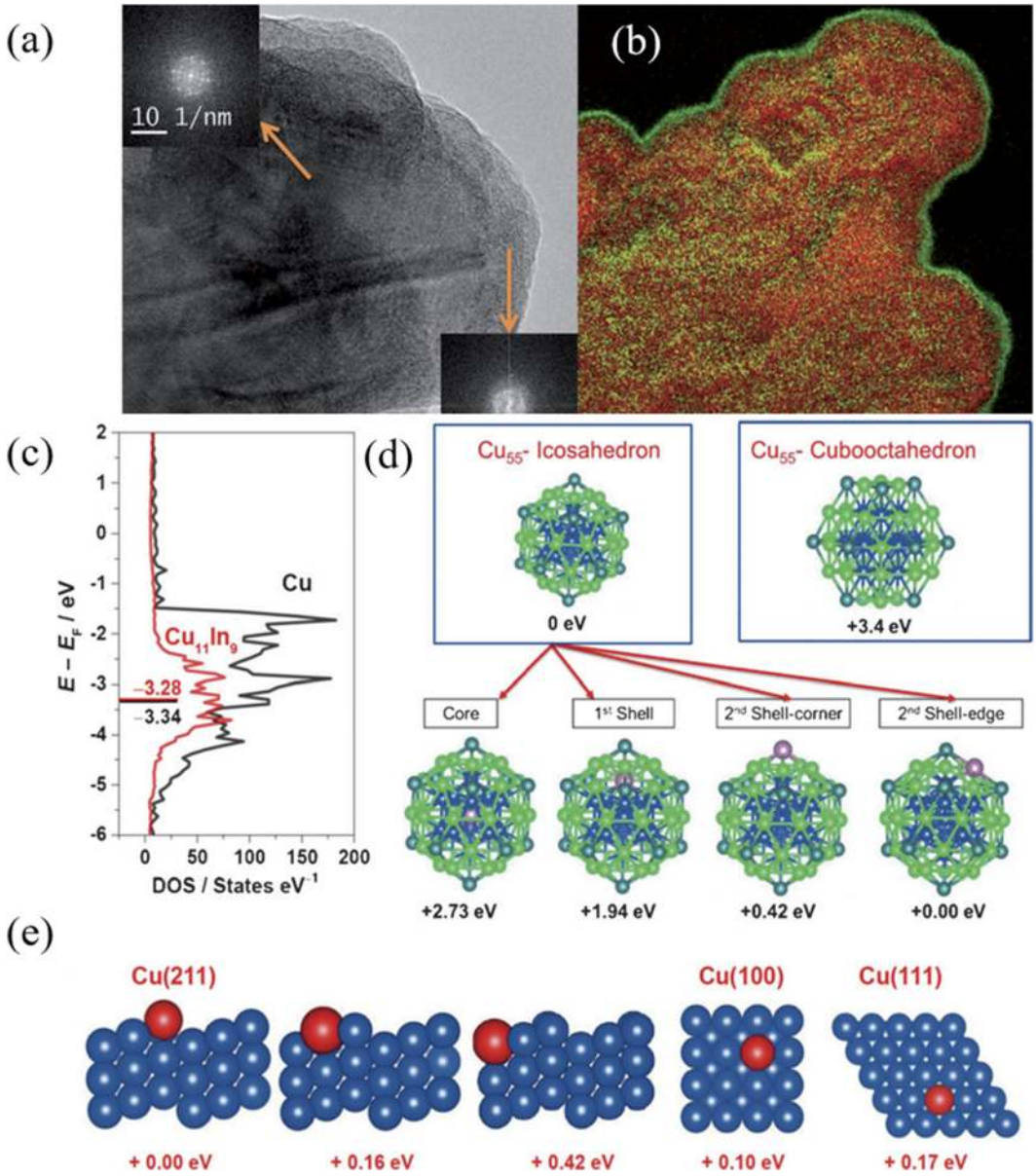

FIG. 13. (a) HR-TEM images of Cu—In with fast Fourier transform (FFT) images from the bulk and the surface (inset). (b) EDS element mapping of the selected area: In (green) and Cu (red). (c) Density of states and value of the d-band center of Cu and of $Cu_{11}In_9$. (d) Site preference and energy change (relative to Cu_{55}—Ih) for replacing one Cu with an In atom in the Cu_{55}-Ih cluster. In the case of Cu_{55}-Oh, the same site preference was obtained for In. (e). Side views of the three possible geometries of the (211) facet and top views of (100) and (111) facet of Cu with one In atom replacing a Cu atom. Adapted with permission from Rasul *et al.*, Angew. Chem., Int. Ed. Engl. **54**, 2146–2150 (2015). Copyright 2015 Wiley-VCH.

Different from Sn-based and In-based electrocatalysts for which the importance and role of metal oxide species in the CO_2RR performance is a matter of general agreement, literature on the active sites and mechanism for Bi-based electrocatalysts are conflicted about whether BiO_x species play a role in the reaction. On one hand, Pander *et al.* analyzed the *in situ* ATR-IR spectra on the Bi surface during CO_2 electrochemical reduction and found that the amount of oxide layer on the Bi surface remains unchanged after initial reduction and no reaction intermediates such as metal-carbonate species (readily observed on Sn- and In-based electrodes) could be detected under working conditions.[242] Based on this spectroscopic evidence, they classified the Bi-electrode as an oxide-independent CO_2RR electrocatalyst.[243] On the other hand, many recent experimental and theoretical reports highlighted the importance of Bi—O

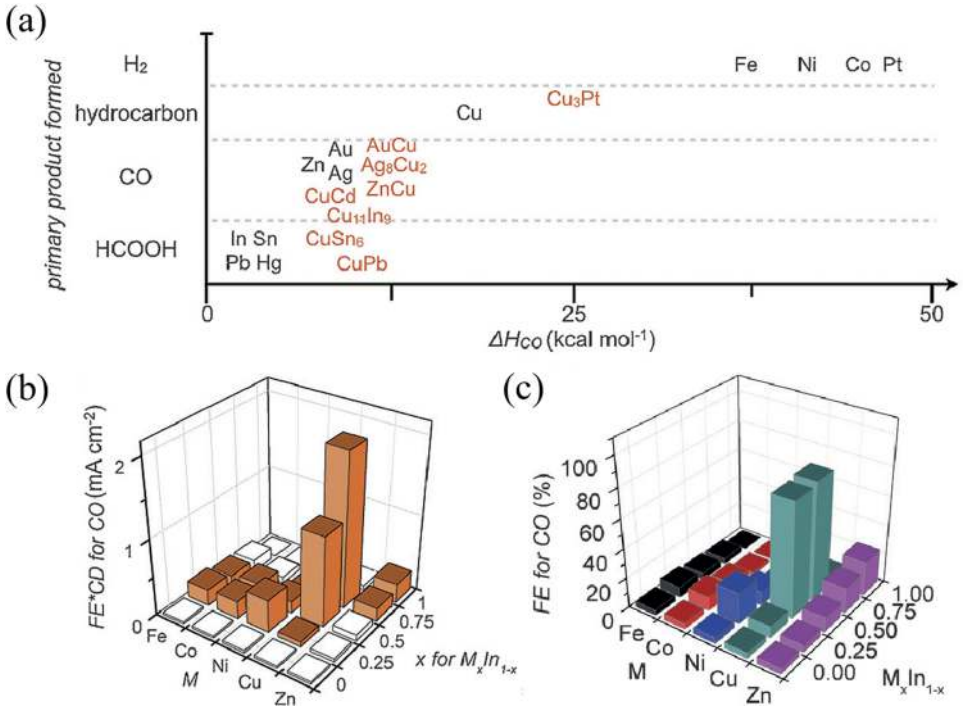

FIG. 14. (a) General relationship between the primary product formed and ΔH_{CO} for metal (black) and bimetallic (orange) CO_2 electrocatalyst films. (b) The partial current for CO at −0.7 V vs RHE for 21 different samples: M_xIn_{1-x} (where M = Co, Ni, Cu, and Zn, x = 0, 0.25, 0.5, and 0.75). (c) CO evolution efficiency at −0.7 V vs RHE for M_xIn_{1-x} (where M = Co, Ni, Cu, and Zn, x = 0, 0.25, 0.5, 0.75, and 1). Reprinted with permission from He *et al.*, Angew. Chem., Int. Ed. Engl. **56**, 6068–6072 (2017). Copyright 2017 Wiley-VCH.

interaction for the performance of Bi-based CO_2RR electrocatalysts. DFT calculations showed that the Bi(111) surface is inert to the adsorption of most species except O_2.[244] Bi—O bonds have stronger stability than Bi—C bonds due to a more effective hybridization between Bi 6s, 6p and O 2p. Therefore, the adsorbates with O—Bi bonds are systematically more stable than those with C—Bi bonds, which results in the stabilization of formate intermediates (*OCHO) over carboxyl intermediates (*COOH), leading to the characteristics

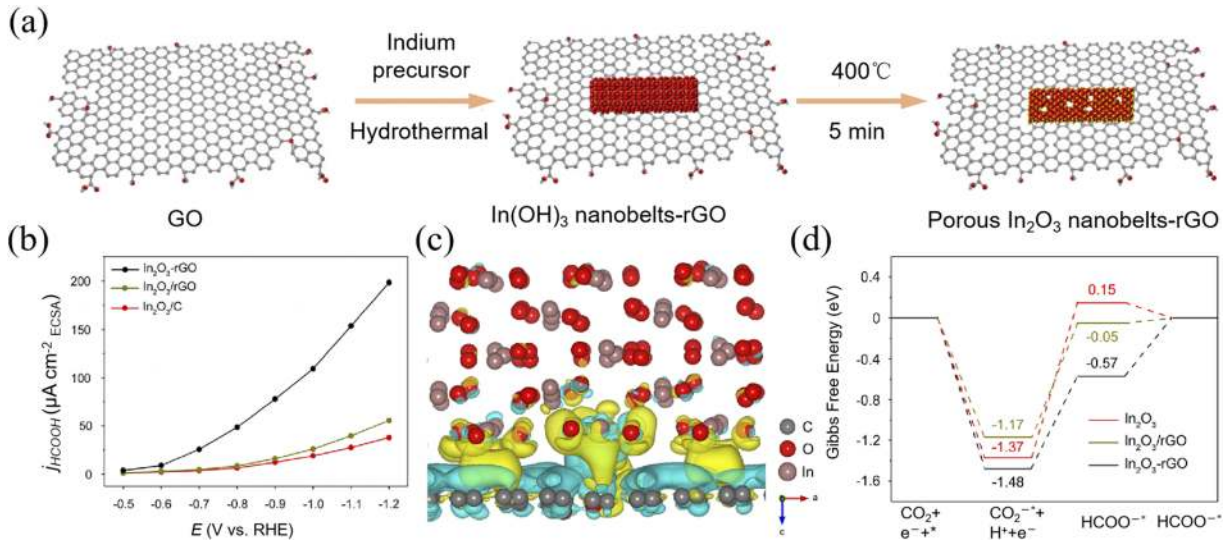

FIG. 15. (a) The preparation process diagram of the In_2O_3—rGO hybrid. (b) The relation plot of ECSA-normalized current density of formate and potential on In_2O_3—rGO hybrid, In_2O_3/rGO, and In_2O_3/C catalysts. (c) The differential charge diagram of the In_2O_3—rGO hybrid catalyst. Yellow represents the electron accumulation area; blue represents the electron loss area. (d) Gibbs free energy diagrams for CO_2 reduction to formate on three catalysts. Adapted with permission from Zhang *et al.*, Nano Lett. **19**, 4029–4034 (2019). Copyright 2019 American Chemical Society.

of the selective formation of HCOOH over CO during the CO_2RR. Some recent experimental and theoretical calculation reports have proposed that Bi^{3+} lone pair electrons in Bi oxides are able to facilitate adsorption and interaction of the catalysts with CO_2.[245–247] The Bi 6s, 6p–O 2p hybridized electronic states make a significant contribution to the top of the valence band in Bi oxides; the energy level and spatial distribution of such electronic states result in the formation of stereochemically active lone pairs that promote electron donation to acidic adsorbed species such as CO_2. In this sense, Deng *et al.* found that the Bi—O structure of bismuth oxides can also accelerate the adsorption and activation of CO_2, switching at the same time the rate-determining step from the initial electron transfer process (to form CO_2^- radicals) to the subsequent protonation step.[237]

2. Morphology and nanostructure engineering

Electrochemical deposition is one of the most common techniques for the preparation of Bi electrodes with different morphologies. Zhong *et al.* studied the effect of addition of KBr into the electrolyte during the electrochemical deposition process.[239] They found that it alters the morphology, particle size, and chemical state of the Bi catalysts, leading to the preparation of dendrite-structured electrocatalysts with large electrochemical surface areas. A maximum FE of 96.4% and a partial current density of 15.2 mA cm^{-2} were achieved at −1.8 V vs SCE in CO_2-saturated 0.5M $NaHCO_3$. Similarly, Koh *et al.* prepared hierarchical Bi dendrites by electrodeposition of the Bi^{3+} precursor in ethylene glycol.[248] The Bi dendrites had superior intrinsic catalytic properties owing to the exposure of high index surfaces with a large amount of undercoordinated sites that were believed to effectively stabilize the *OCHO intermediate. As a result, it exhibited the maximum formate FE of about 89% at −0.74 V vs RHE.

2D Bi nanosheets are widely studied catalyst structures because it often leads to improved performances and there are numerous synthetic techniques to obtain such a structure. Bulk Bi has a layered structure isomorph like black phosphorus that can be exfoliated to form 2D (nanosheets) structures by the so-called liquid-phase exfoliation. Zhang *et al.* used this technique to prepare ultrathin 2D Bi nanosheets, which were shown to have improved performances as compared with the bulk Bi electrode. Exfoliated nanosheets presented the enhanced formate FE of 86% and a current density of 16.5 mA cm^{-2} at −1.1 V vs RHE in CO_2-saturated 0.1M $KHCO_3$.[249] DFT calculations revealed that the edge sites can more effectively stabilize the formation of the *OCHO intermediate and are, therefore, the preferred active sites. Ultra-thin Bi nanosheets (about 10 nm) with numerous low-coordination sites have been fabricated through hydrothermal treatment of the electrodeposited Bi-electrode.[250] The performance of the nanosheet structured electrocatalysts featured a formate FE higher than 90% in a potential range from −0.9 V to −1.2 V vs RHE, achieving current densities around 14 mA cm^{-2}. The authors argued that the improved catalytic performance was attributed to a higher partial density of states of the Bi p band around the Fermi level, which usually facilitates the orbital hybridization of the catalyst with adsorbed reactants.

Metallic Bi nanosheets can also be prepared through topotactic transformation of Bi compounds such as layered Bi oxyhalides (BiOI[251] and BiOBr[252]) and layer carbonate ($Bi_2O_2CO_3$).[33] For example, Li and co-workers prepared BiOI nanosheets and found that the nanosheet structure was maintained when BiOI was cathodically reduced to metallic Bi. The Bi nanosheets can catalyze the CO_2RR to formate with an excellent selectivity of >90% and a large partial current density of 24 mA cm^{-2} at −1.74 V vs SCE. Although, in principle, it is possible to prepare Bi monolayers, it has been theoretically demonstrated that for Bi nanosheets, it is not always "the thinner the better."[253] Due to the existence of a sizable bandgap, the Bi monolayer exhibits lower catalytic activity than thicker metallic Bi nanosheets in a microkinetic model of CO_2 conversion to HCOOH.

Introducing structure disorders or defects can also provide local electronic states, which may have a positive impact on the stabilization of reaction intermediates.[254,255] For example, Li and co-workers prepared Bi nanoparticles/Bi_2O_3 nanosheets with abundant GBs through a controlled hydrothermal route.[256] A large partial current density for formate (24.4 mA cm^{-2}) and high FE (>90%) for formate under a wide potential range have been achieved, which was ascribed to the intermediate stabilization effects associated with GBs. In another work, Gong *et al.* prepared defective Bi/Bi_2O_3 nanotubes, which showed 60 mA cm^{-1} of formate partial current density at −1.05 V vs RHE in 0.5M CO_2-saturated $KHCO_3$ solution.[254] DFT calculations suggested that structural defects (e.g., Bi vacancies) can boost the electrocatalytic performance by stabilizing *OCHO intermediates. Moreover, this catalyst can achieve a large current density of 288 mA cm^{-1} at −0.61 V vs RHE in 1M KOH when used in a flow cell reactor. The large current density is larger than commercial standards (>200 mA cm^{-1}).

3. Doping and alloying

The intrinsic CO_2 reduction activity of Bi electrodes has been shown to benefit from the formation of alloys with other metals and advanced composite structures.[257,258] Hoffman *et al.* studied the electrochemical reduction of CO_2 at dendritic Cu, Bi, and Cu—Bi alloys with varying compositions.[258] Due to the crystal lattice and symmetry mismatch between Cu and Bi, the dendritic structures of the alloys displayed a high density of defect sites, which serve as active catalytic sites. The catalytic properties of bimetallic Cu—Bi catalysts could be effectively tuned upon varying the composition, reaching a maximum of 90% formate FE at around −0.85 V vs RHE for 40–60 at. % Bi concentration. The authors argued that the modulation of catalytic properties originated from the adjustment of the relative adsorption strength of reaction intermediates.

Bi—Sn metallic composites have also been shown to yield high selectivity and stability for CO_2 reduction. Owing to the formation of active sites through favorable orbital interactions at the Sn—Bi interface, a Bi—Sn bimetallic catalyst converted CO_2 to formate with 96% FE and production rate of 0.74 mmol h^{-1} cm^{-2} at −1.1 V vs RHE.[203] DFT simulation showed that at the Bi—Sn interface, p and d orbitals of Sn electron states upshift away from the Fermi level, leading to the shifting of the electron density from more electronegative O atoms to the p and d orbitals of Sn atoms. This increases the stability of *OCHO intermediates on Bi—Sn surfaces compared with pure Sn or Bi, resulting in better catalytic properties (Fig. 16).[203]

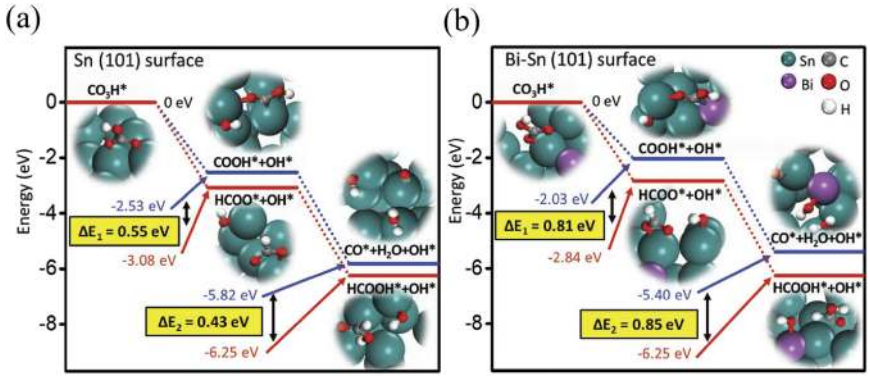

FIG. 16. Schematic diagram of energy profiles for the CO_2RR to generate CO (top) and HCOOH (bottom) on the (a) Sn (101) surface and (b) Bi—Sn (101) surface. All energies are with reference to the energies of CO_2H adsorbed on the Sn (101) or Bi—Sn (101) surface. Reprinted with permission from Wen *et al.*, Adv. Energy Mater. **8**, 1802427 (2018). Copyright 2018 Wiley-VCH.

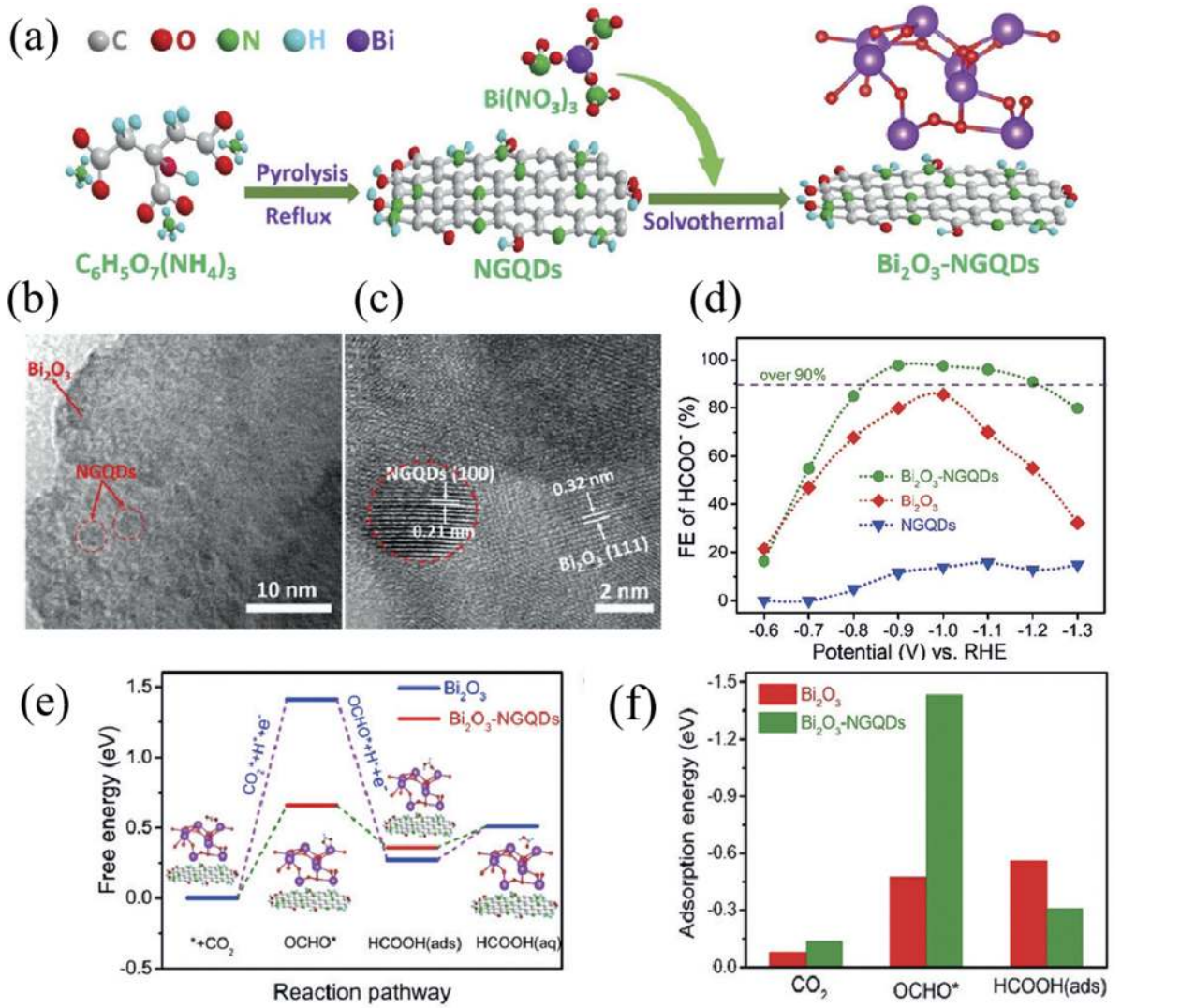

FIG. 17. (a) Schematic of the synthesis process for Bi_2O_3-NGQDs. (b) TEM and (c) HRTEM images for Bi_2O_3-NGQDs. (d) FE of formate for Bi_2O_3-NGQDs, Bi_2O_3, and NGQDs at different electrolytic potentials. (e) Free-energy diagram and (f) adsorption energy of CO_2, OCHO*, and HCOOH(ads). Adapted with permission from Chen *et al.*, Angew. Chem., Int. Ed. Engl. **57**, 12790–12794 (2018). Copyright 2018 Wiley-VCH.

Moreover, Bi-graphene composites have been shown to improve the CO_2 adsorption capacity, which alleviates problems related to the weak adsorption of CO_2 and mass transport limitations, characteristic of the CO_2 reduction process. Chen *et al.* synthesized a composite structure of Bi_2O_3 nanosheets and N-doped graphene quantum dots (NGQDs) by a simple solvothermal method (Fig. 17).[259] They showed that these materials are able to promote the CO_2 reduction at an average formate FE of 95.6% in the range of −0.9 V to −1.2 V vs RHE. DFT calculations revealed that increased adsorption energy of CO_2 and the OCHO* intermediate, promoted by NGQDs, results in the enhanced performance of nanostructured Bi_2O_3 catalysts.

D. Lead-based electrocatalysts

1. Active sites and reaction mechanism

Despite its well-known toxicity, the mechanism of Pb-based electrocatalysts for CO_2 reduction to formate is worth exploring. Although the overpotentials required to drive the reaction on Pb electrodes are usually higher than those required with other p-block electrodes, high formate FE (~95%) is usually obtained.[62,260–262] Early mechanistic studies based on DFT calculations suggested that the origin of the characteristic high selectivity of the Pb electrocatalyst for HCOOH production (over CO and H_2) lies in the strong O-affinitive and weak C-, H-affinitive characteristics of Pb, which leads to the involvement of the *OCHO species as a key intermediate to produce HCOOH exclusively, preventing unwanted H_2 production at the same time.[129,263] However, later DFT calculations considered the effects of the formation of the solvent and cations in the electrolyte and suggested that the reaction may preferentially proceed via direct carbon-bond *COOH intermediates, which have the same high formate selectivity.[264]

In fact, experimental mechanistic studies based on *in situ* ATR-IR carried out by Pander *et al.* showed that the CO_2 reduction on Pb electrodes did not proceed through the formation of Pb carbonates, which suggests that the reaction occurs on pure metallic Pb surfaces via direct carbon-bond *COOH intermediates.[242] However, the author reported that the total faradaic yield for formate production increased upon anodization of the electrode surface, suggesting that surface oxide species improve the performance of Pb electrodes. Lee and Kanan reported a similar observation on nanocrystalline Pb films prepared by reducing PbO_2 precursors had a significant higher formate FE than that of polycrystalline Pb foil electrodes.[260]

2. Nanostructure engineering and alloying

Despite Pb-based electrocatalysts have excellent selectivity for formate formation, the intrinsic toxicity and concomitant environmental unfriendliness make this material not ideal for electrochemical CO_2 reduction, and as a result, it has gained less attention than other p-block metals. There is only a small amount of studies on the nanostructuring and doping of Pb-based electrodes such as plate, nanowires, nanoparticles, sulfide-derived Pb, and oxide-derived Pb.[34,35,265–267] Their catalytic properties, especially FE, have a close relationship with nanostructures, morphologies, crystalline structures, and composition effects of Pb electrodes. For example, the Pb electrodes with the wafer structures show the enhanced selectivity of formate.[266] Fan *et al.* fabricated lead electrodes with a honeycomb primary structure and a dendrite-like secondary structure grown along the [100]-axis. Such a structure was shown to supply abundant electrode/electrolyte contact surface area and strong structural stability for the CO_2RR.[261] Additionally, the tip closed by [111] planes showed local high fields, which results in a high concentration of CO_2 on the tip surface, which was beneficial to improve the reaction rate and decrease the overpotential. An FE of 97% and a partial current density of −7.5 mA cm^{-1} for formate production were achieved under the potential of −0.99 V vs RHE that was stable for more than 6 h.

In terms of the influence of composition, Choi *et al.* notably showed that the Sn—Pb alloy surface led to higher electrical conductivity and stronger electron-donating ability compared to the single metal electrode. These effects were ascribed to the formation of SnO_x and Pb^0 on the alloy surface.[204] It was shown that the presence of Pb (15–35 at. %) had the ability to stabilize SnO_2.[265] At the same time, the alloy composition may supply synergistic catalytic effects on selective adsorption sites and electronic interactions.[265,268]

IV. SUMMARY AND PERSPECTIVE

In this article, we provide a review on the recent developments and understanding of the p-block metal-based (Sn, In, Bi, and Pb) electrocatalysts for electrochemical CO_2 reduction. This unique group of electrocatalysts has been shown to drive CO_2 reduction to formate with a particularly high FE well above 90%. This is fundamentally governed by the unique surface physicochemical properties of this group of materials, which favorably stabilize the *OCHO intermediate to form formate, and at the same time, they are unfavorable for the formation of *COOH (intermediate to CO or CH_4) or *H (intermediate to H_2). We focus on the fundamental understanding of surface chemistry, active sites, and structure–activity relationships. Strategies to enhance the activity including morphology control, nanostructuring, grain boundaries, doping, alloying, and defect engineering are briefly reviewed.

Regarding the active sites for the CO_2RR, a key observation is that the presence of metal oxide species on the catalyst surfaces under the electrochemical CO_2RR conditions is crucial for the activity and selectivity of Sn and In based electrocatalysts. The persistence of oxide species can be rationalized on the basis of the oxophilicity of p-block metals, which is considered to be moderate in a quantitative scale of oxophilicity.[269] Inferred from *in situ* spectroscopic studies, the p-block metal oxides might provide surface basicity for the chemisorption of acidic CO_2 molecules to form surface bound metal carbonates. Furthermore, the oxide species may also facilitate electron transfer to the stabilized CO_2^- intermediate, which is regarded as the RDS for the CO_2RR. Now, it is interesting to ask the question: how the CO_2 molecule or other reaction intermediates interact with the catalyst surface. Previous studies on the surface chemistry of p-block metal oxides indicated that the p-block metal is dominated by the group oxidation state N and a lower N-2 oxidation state, which is associated with the occupation of a metal s^2 lone pair, as found in compounds of Sn^{2+}, Bi^{3+}, Pb^{2+}, and In^+ on the surface of In_2O_3.[287] Lone pairs project out of the surface, hence providing localized surface electron density where for the chemisorption of CO_2.[247,270,271] Therefore, more detailed research on the role

of surface oxides may lead to important design guidelines to maximize both the intrinsic and overall performances of p-block metal catalysts for CO_2 reduction.

Mechanistic studies have been largely based on DFT calculations. It has been found that there is a strong correlation between the DFT calculated *OCHO binding energies and the experimentally reported activities of different electrocatalysts, which have led to the conclusion that *OCHO, the key intermediate for formate formation. However, it should be noted that the catalyst surfaces (i.e., metallic Sn) used for DFT calculations are different from the real surfaces with oxide species observed experimentally. *In operando* characterizations suggest that the surface-bound metal carbonate is a crucial reaction intermediate for transforming CO_2 into formate. The situation is further complicated by the dynamic behavior of the catalyst composition during the reduction reaction conditions with multiple oxidation states present under different reaction conditions. At present, it is still not well understood the role of oxide species in the reaction pathway and mechanism for the CO_2RR to formate. Therefore, combining theoretical calculations with "actual" reaction intermediates evidenced from *in operando* characterizations, such as infrared spectroscopy, Raman spectroscopy, and XAS under working conditions, is particularly important in order to elucidate the reaction mechanism.

Significant progress has been made for the development of new electrocatalysts with better selectivity, activity, and stability. Many strategies including morphology control, surface modification, nanostructuring, grain boundaries, doping, alloying, and defect engineering have been adopted to synthesize a variety of materials. The goals of these methods are to increase their active site density and/or to promote their site-specific activity, but at this stage they are still based on a trial-and-error approach. It is straightforward to understand that shrinking the dimensions and sizes of electrocatalysts can create more active sites on the surface for electrochemical reactions. Meanwhile, nanostructuring may also introduce new reaction sites, such as preferential exposure of different crystal facets, more atoms with coordinately unsaturated sites at steps and edges, and structural defects such as vacancies and GBs that may afford unexpected electrocatalytic activities. However, how these new reaction sites impact the electrocatalytic performance (i.e., structure–activity relation), which is essential for rational design of better catalysts, remains to be answered.

On the other hand, a standard procedure for measurements and comparisons is still needed. The nanostructured materials prepared by different scientific groups usually have different surface areas, which complicates the comparison of a fair evaluation of relevance of the particular material properties for the CO_2RR. Additionally, the CO_2RR performance assessment is further complicated by the complex methods of measurement, which can be altered by even the trace amount of impurity in the electrolyte. In this sense, compared with ill-defined porous electrodes commonly used in CO_2RR studies, single crystal thin films permit a high degree of control over crystal facets, defects, and compositions, which could be used as a model catalyst to gain a definitive structure–property relationship at a molecular level.

Doping and alloying with foreign atoms can induce a significant change in the electronic properties and are the most effective ways to develop a new electrocatalyst. Electronic structure parameters such as the density of state near the Fermi level dictate the binding strength with reaction intermediates and hence the activation barrier for the reaction.[247,272,273,288] However, so far there is still a lack of understanding of how doping, alloying, or defects influence the electronic structure and its relationship with CO_2RR selectivity and activity. Moreover, alloying to form bimetallic or ternary catalysts could offer synergistic effects from different active sites and hold the potential to significantly alter the selectivity and activity. For example, as discussed above, alloying Sn with Cu and Ag can enhance the selectivity for formate, while alloying In with Cu alter the selectivity to CO. Furthermore, theoretical studies indicated that scaling relations that exist between adsorption energies of different reaction intermediates can be tailored by alloying or doping. Therefore, a deeper insight into catalytic reaction pathways involving scaling relations among reactive intermediates and structure–property relationships is highly needed as "descriptors" for the rational design of highly active catalysts with better selectivity and stability.

ACKNOWLEDGMENTS

K. H. L. Zhang is grateful for funding from the National Natural Science Foundation of China (Grant No. 21872116) and funding for the "single-crystal electrochemistry" project from the State Key Laboratory of Physical Chemistry of Solid Surfaces.

REFERENCES

[1] N. S. Lewis and D. G. Nocera, "Powering the planet: Chemical challenges in solar energy utilization," Proc. Natl. Acad. Sci. U. S. A **103**, 15729–15735 (2006).
[2] S. Chu and A. Majumdar, "Opportunities and challenges for a sustainable energy future," Nature **488**, 294–303 (2012).
[3] M. Mikkelsen, M. Jørgensen, and F. C. Krebs, "The teraton challenge. A review of fixation and transformation of carbon dioxide," Energy Environ. Sci. **3**, 43–81 (2010).
[4] C. Vogt, M. Monai, G. J. Kramer, and B. M. Weckhuysen, "The renaissance of the Sabatier reaction and its applications on Earth and in space," Nat. Catal. **2**, 188–197 (2019).
[5] C. Hepburn, E. Adlen, and J. Beddington, "The technological and economic prospects for CO_2 utilization and removal," Nature **575**, 87–97 (2019).
[6] P. Gao, S. Li, and X. Bu, "Direct conversion of CO_2 into liquid fuels with high selectivity over a bifunctional catalyst," Nat. Chem. **9**, 1019–1024 (2017).
[7] J. Wang, G. Li, and Z. Li, "A highly selective and stable ZnO–ZrO_2 solid solution catalyst for CO_2 hydrogenation to methanol," Sci. Adv. **3**, e1701290 (2017).
[8] W. Li, H. Wang, and X. Jiang, "A short review of recent advances in CO_2 hydrogenation to hydrocarbons over heterogeneous catalysts," RSC Adv. **8**, 7651–7669 (2018).
[9] J. Yu, J. Low, W. Xiao, P. Zhou, and M. Jaroniec, "Enhanced photocatalytic CO_2-reduction activity of anatase TiO_2 by Co-exposed {001} and {101} facets," J. Am. Chem. Soc. **136**, 8839–8842 (2014).
[10] X. Chang, T. Wang, and J. Gong, "CO_2 photo-reduction: Insights into CO_2 activation and reaction on surfaces of photocatalysts," Energy Environ. Sci. **9**, 2177–2196 (2016).
[11] J. Low, B. Cheng, and J. Yu, "Surface modification and enhanced photocatalytic CO_2 reduction performance of TiO_2: A review," Appl. Surf. Sci. **392**, 658–686 (2017).
[12] J. Xiong, J. Di, J. Xia, W. Zhu, and H. Li, "Surface defect engineering in 2D nanomaterials for photocatalysis," Adv. Funct. Mater. **28**, 1801983 (2018).

[13]Q. Han, X. Bai, Z. Man, and H. He, "Convincing synthesis of atomically thin, single-crystalline $InVO_4$ sheets toward promoting highly selective and efficient solar conversion of CO_2 into CO," J. Am. Chem. Soc. **141**, 4209–4213 (2019).
[14]Y. Zhao, G. I. N. Waterhouse, and G. Chen, "Two-dimensional-related catalytic materials for solar-driven conversion of CO_x into valuable chemical feedstocks," Chem. Soc. Rev. **48**, 1972–2010 (2019).
[15]A. Vasileff, Y. Zheng, and S. Z. Qiao, "Carbon solving carbon's problems: Recent progress of nanostructured carbon-based catalysts for the electrochemical reduction of CO_2," Adv. Energy Mater. **7**, 1700759 (2017).
[16]Z. Sun, T. Ma, H. Tao, Q. Fan, and B. Han, "Fundamentals and challenges of electrochemical CO_2 reduction using two-dimensional materials," Chem **3**, 560–587 (2017).
[17]L. Zhang, Z.-J. Zhao, and J. Gong, "Nanostructured materials for heterogeneous electrocatalytic CO_2 reduction and their related reaction mechanisms," Angew. Chem., Int. Ed. Engl. **56**, 11326–11353 (2017).
[18]J. Wu, Y. Huang, W. Ye, and Y. Li, "CO_2 reduction: From the electrochemical to photochemical approach," Adv. Sci. **4**, 1700194 (2017).
[19]J. Gan, X. Lu, J. Wu, and S. Xie, "Oxygen vacancies promoting photoelectrochemical performance of In_2O_3 nanocubes," Sci. Rep. **3**, 1021 (2013).
[20]M. Schreier, L. Curvat, and F. Giordano, "Efficient photosynthesis of carbon monoxide from CO_2 using perovskite photovoltaics," Nat. Commun. **6**, 7326 (2015).
[21]S. Chu, P. Ou, P. Ghamari, and S. Vanka, "Photoelectrochemical CO_2 reduction into syngas with the metal/oxide interface," J. Am. Chem. Soc. **140**, 7869–7877 (2018).
[22]S. Xu and E. A. Carter, "Theoretical insights into heterogeneous (photo) electrochemical CO_2 reduction," Chem. Rev. **119**, 6631–6669 (2019).
[23]Q. Li, J. Fu, W. Zhu, Z. Chen, and S. Sun, "Tuning Sn-catalysis for electrochemical reduction of CO_2 to CO via the core/shell Cu/SnO_2 structure," J. Am. Chem. Soc. **139**, 4290–4293 (2017).
[24]X. Bai, W. Chen, and C. Zhao, "Exclusive formation of formic acid from CO_2 electroreduction by a tunable Pd–Sn alloy," Angew. Chem., Int. Ed. Engl. **56**, 12219–12223 (2017).
[25]R. L. Machunda, H. Ju, and J. Lee, "Electrocatalytic reduction of CO_2 gas at Sn based gas diffusion electrode," Curr. Appl. Phys. **11**, 986–988 (2011).
[26]C. Zhao and J. Wang, "Electrochemical reduction of CO_2 to formate in aqueous solution using electro-deposited," Chem. Eng. J. **293**, 161–170 (2016).
[27]Z. Xia, M. Freeman, and D. Zhang, "Highly selective electrochemical conversion of CO_2 to HCOOH on dendritic indium foams," ChemElectroChem **5**, 253–259 (2018).
[28]S. Wang, B. Y. Guan, and X. W. D. Lou, "Construction of $ZnIn_2S_4$–In_2O_3 hierarchical tubular heterostructures for efficient CO_2 photoreduction," J. Am. Chem. Soc. **140**, 5037–5040 (2018).
[29]M. Tahir and N. S. Amin, "Indium-doped TiO_2 nanoparticles for photocatalytic CO_2 reduction with H_2O vapors to CH_4," Appl. Catal., B **162**, 98–109 (2015).
[30]Z. M. Detweiler, J. L. White, S. L. Bernasek, and A. B. Bocarsly, "Anodized indium metal electrodes for enhanced carbon dioxide reduction in aqueous electrolyte," Langmuir **30**, 7593–7600 (2014).
[31]X. Zhang, T. Lei, Y. Liu, and J. Qiao, "Enhancing CO_2 electrolysis to formate on facilely synthesized Bi catalysts at low overpotential," Appl. Catal., B **218**, 46–50 (2017).
[32]Z. Zhang, M. Chi, and G. M. Veith, "Rational design of Bi nanoparticles for efficient electrochemical CO_2 reduction: The elucidation of size and surface condition effects," ACS Catal. **6**, 6255–6264 (2016).
[33]H. Yang, N. Han, J. Deng, and J. Wu, "Selective CO_2 reduction on 2D mesoporous Bi nanosheets," Adv. Energy Mater. **8**, 1801536 (2018).
[34]Y. Kwon and J. Lee, "Formic acid from carbon dioxide on nanolayered electrocatalyst," Electrocatalysis **1**, 108–115 (2010).
[35]Z. He, J. Shen, and Z. Ni, "Electrochemically created roughened lead plate for electrochemical reduction of aqueous CO_2," Catal. Commun. **72**, 38–42 (2015).
[36]T. Ma, Q. Fan, and H. Tao, "Heterogeneous electrochemical CO_2 reduction using nonmetallic carbon-based catalysts: Current status and future challenges," Nanotechnology **28**, 472001 (2017).
[37]S. Zhang, P. Kang, and S. Ubnoske, "Polyethylenimine-enhanced electrocatalytic reduction of CO_2 to formate at nitrogen-doped carbon nanomaterials," J. Am. Chem. Soc. **136**, 7845–7848 (2014).
[38]Z. Chen, K. Mou, S. Yao, and L. Liu, "Highly selective electrochemical reduction of CO_2 to formate on metal-free nitrogen-doped PC61BM," J. Mater. Chem. A **6**, 11236–11243 (2018).
[39]H.-R. M. Jhong, S. Ma, and P. J. A. Kenis, "Electrochemical conversion of CO_2 to useful chemicals: Current status, remaining challenges, and future opportunities," Curr. Opin. Chem. Eng. **2**, 191–199 (2013).
[40]J.-P. Jones, G. K. S. Prakash, and G. A. Olah, "Electrochemical CO_2 reduction: Recent advances and current trends," Isr. J. Chem. **54**, 1451–1466 (2014).
[41]Q. Lu, J. Rosen, and F. Jiao, "Nanostructured metallic electrocatalysts for carbon dioxide reduction," ChemCatChem. **7**, 38–47 (2015).
[42]B. Kumar, J. P. Brian, and V. Atla, "New trends in the development of heterogeneous catalysts for electrochemical CO_2 reduction," Catal. Today **270**, 19–30 (2016).
[43]Q. Lu and F. Jiao, "Electrochemical CO_2 reduction: Electrocatalyst, reaction mechanism, and process engineering," Nano Energy **29**, 439–456 (2016).
[44]J. J. Carroll, J. D. Slupsky, and A. E. Mather, "The solubility of carbon dioxide in water at low pressure," J. Phys. Chem. Ref. Data **20**, 1201–1209 (1991).
[45]A. Del Castillo, M. Alvarez-Guerra, and A. Irabien, "Continuous electroreduction of CO_2 to formate using Sn gas diffusion electrodes," AIChE J. **60**, 3557–3564 (2014).
[46]D. A. Salvatore, D. M. Weekes, and J. He, "Electrolysis of gaseous CO_2 to CO in a flow cell with a bipolar membrane," ACS Energy Lett. **3**, 149–154 (2017).
[47]D. M. Weekes, D. A. Salvatore, A. Reyes, A. Huang, and C. P. Berlinguette, "Electrolytic CO_2 reduction in a flow cell," Acc. Chem. Res. **51**, 910–918 (2018).
[48]P. Jeanty, C. Scherer, and E. Magori, "Upscaling and continuous operation of electrochemical CO_2 to CO conversion in aqueous solutions on silver gas diffusion electrodes," J. CO_2 Util. **24**, 454–462 (2018).
[49]S. Ren, D. Joulié, and D. Salvatore, "Molecular electrocatalysts can mediate fast, selective CO_2 reduction in a flow cell," Science **365**, 367–369 (2019).
[50]J. Medina-Ramos, R. C. Pupillo, T. P. Keane, J. L. DiMeglio, and J. Rosenthal, "Efficient conversion of CO_2 to CO using tin and other inexpensive and easily prepared post-transition metal catalysts," J. Am. Chem. Soc. **137**, 5021–5027 (2015).
[51]S. Kaneco, K. Iiba, H. Katsumata, T. Suzuki, and K. Ohta, "Effect of sodium cation on the electrochemical reduction of CO_2 at a copper electrode in methanol," J. Solid State Electr. **11**, 490–495 (2006).
[52]B. A. Rosen, A. Salehi-Khojin, and M. R. Thorson, "Ionic liquid-mediated selective conversion of CO_2 to CO at low overpotentials," Science **334**, 643–644 (2011).
[53]J. L. DiMeglio and J. Rosenthal, "Selective conversion of CO_2 to CO with high efficiency using an inexpensive bismuth-based electrocatalyst," J. Am. Chem. Soc. **135**, 8798–8801 (2013).
[54]Y. Wang, P. Han, X. Lv, L. Zhang, and G. Zheng, "Defect and interface engineering for aqueous electrocatalytic CO_2 reduction," Joule **2**, 2551–2582 (2018).
[55]G. Glockler, "Carbon–Oxygen bond energies and bond distances," J. Phys. Chem. **62**, 1049–1054 (1958).
[56]H. A. Schwarz and R. W. Dodson, "Reduction potentials of CO_2^- and the alcohol radicals," J. Phys. Chem. **93**, 409–414 (1989).
[57]E. E. Benson, C. P. Kubiak, A. J. Sathrum, and J. M. Smieja, "Electrocatalytic and homogeneous approaches to conversion of CO_2 to liquid fuels," Chem. Soc. Rev. **38**, 89–99 (2009).
[58]J. Qiao, Y. Liu, F. Hong, and J. Zhang, "A review of catalysts for the electroreduction of carbon dioxide to produce low-carbon fuels," Chem. Soc. Rev. **43**, 631–675 (2014).
[59]Y. Hori, "Electrochemical CO_2 reduction on metal electrodes," *Modern Aspects of Electrochemistry* (Springer, New York, NY, 2008), pp. 89–189.
[60]Y.-J. Zhang, V. Sethuraman, R. Michalsky, and A. A. Peterson, "Competition between CO_2 reduction and H_2 evolution on transition-metal electrocatalysts," ACS Catal. **4**, 3742–3748 (2014).
[61]Y. Hori, H. Wakebe, T. Tsukamoto, and O. Koga, "Electrocatalytic process of CO selectivity in electrochemical reduction of CO_2 at metal electrodes in aqueous media," Electrochim. Acta **39**, 1833–1839 (1994).

[62]Y. Hori, K. Kikuchi, and S. Suzuki, "Production of CO and CH_4 in electrochemical reduction of CO_2 at metal electrodes in aqueous hydrogencarbonate solution," Chem. Lett. **14**, 1695–1698 (1985).
[63]Y. Hori and A. Murata, "Electrochemical evidence of intermediate formation of adsorbed CO in cathodic reduction of CO_2 at a nickel electrode," Electrochim. Acta **35**, 1777–1780 (1990).
[64]H. A. Hansen, J. B. Varley, A. A. Peterson, and J. K. Nørskov, "Understanding trends in the electrocatalytic activity of metals and enzymes for CO_2 reduction to CO," J. Phys. Chem. Lett. **4**, 388–392 (2013).
[65]D. T. Whipple and P. J. A. Kenis, "Prospects of CO_2 utilization via direct heterogeneous electrochemical reduction," J. Phys. Chem. Lett. **1**, 3451–3458 (2010).
[66]C. Costentin, M. Robert, and J.-M. Savéant, "Catalysis of the electrochemical reduction of carbon dioxide," Chem. Soc. Rev. **42**, 2423–2436 (2013).
[67]H. Xie, T. Wang, J. Liang, Q. Li, and S. Sun, "Cu-based nanocatalysts for electrochemical reduction of CO_2," Nano Today **21**, 41–54 (2018).
[68]A. A. Peterson, F. Abild-Pedersen, F. Studt, J. Rossmeisl, and J. K. Nørskov, "How copper catalyzes the electroreduction of carbon dioxide into hydrocarbon fuels," Energy Environ. Sci. **3**, 1311–1315 (2010).
[69]R. Kortlever, J. Shen, K. J. Schouten, F. Calle-Vallejo, and M. T. Koper, "Catalysts and reaction pathways for the electrochemical reduction of carbon dioxide," J. Phys. Chem. Lett. **6**, 4073–4082 (2015).
[70]M. B. Ross, P. De Luna, and Y. Li, "Designing materials for electrochemical carbon dioxide recycling," Nat. Catal. **2**, 648–658 (2019).
[71]Z. W. Seh, J. Kibsgaard, and C. F. Dickens, "Combining theory and experiment in electrocatalysis: Insights into materials design," Science **355**, 4998 (2017).
[72]A. J. Welch, J. S. DuChene, and G. Tagliabue, "Nanoporous gold as a highly selective and active carbon dioxide reduction catalyst," ACS Appl. Energy Mater. **2**, 164–170 (2018).
[73]W. Zhu, Y.-J. Zhang, and H. Zhang, "Active and selective conversion of CO_2 to CO on ultrathin Au nanowires," J. Am. Chem. Soc. **136**, 16132–16135 (2014).
[74]Y. Chen, C. W. Li, and M. W. Kanan, "Aqueous CO_2 reduction at very low overpotential on oxide-derived Au nanoparticles," J. Am. Chem. Soc. **134**, 19969–19972 (2012).
[75]S. Back, M. S. Yeom, and Y. Jung, "Active sites of Au and Ag nanoparticle catalysts for CO_2 electroreduction to CO," ACS Catal. **5**, 5089–5096 (2015).
[76]E. R. Cave, J. H. Montoya, and K. P. Kuhl, "Electrochemical CO_2 reduction on Au surfaces: Mechanistic aspects regarding the formation of major and minor products," Phys. Chem. Chem. Phys. **19**, 15856–15863 (2017).
[77]B. Kim, S. Ma, H.-R. Molly Jhong, and P. J. A. Kenis, "Influence of dilute feed and pH on electrochemical reduction of CO_2 to CO on Ag in a continuous flow electrolyzer," Electrochim. Acta **166**, 271–276 (2015).
[78]C. Kim, H. S. Jeon, and T. Eom, "Achieving selective and efficient electrocatalytic activity for CO_2 reduction using immobilized silver nanoparticles," J. Am. Chem. Soc. **137**, 13844–13850 (2015).
[79]J. Rosen, G. S. Hutchings, and Q. Lu, "Mechanistic insights into the electrochemical reduction of CO_2 to CO on nanostructured Ag surfaces," ACS Catal. **5**, 4293–4299 (2015).
[80]M. R. Singh, Y. Kwon, Y. Lum, J. W. Ager, and A. T. Bell, "Hydrolysis of electrolyte cations enhances the electrochemical reduction of CO_2 over Ag and Cu," J. Am. Chem. Soc. **138**, 13006–13012 (2016).
[81]T. Hatsukade, K. P. Kuhl, E. R. Cave, D. N. Abram, and T. F. Jaramillo, "Insights into the electrocatalytic reduction of CO_2 on metallic silver surfaces," Phys. Chem. Chem. Phys. **16**, 13814–13819 (2014).
[82]H. S. Jeon, I. Sinev, and F. Scholten, "Operando evolution of the structure and oxidation state of size-controlled Zn nanoparticles during CO_2 electroreduction," J. Am. Chem. Soc. **140**, 9383–9386 (2018).
[83]J. Rosen, G. S. Hutchings, and Q. Lu, "Electrodeposited Zn dendrites with enhanced CO selectivity for electrocatalytic CO_2 reduction," ACS Catal. **5**, 4586–4591 (2015).
[84]H. Won da, H. Shin, and J. Koh, "Highly efficient, selective, and stable CO_2 electroreduction on a hexagonal Zn catalyst," Angew. Chem., Int. Ed. Engl. **55**, 9297–9300 (2016).
[85]Z. Geng, X. Kong, and W. Chen, "Oxygen vacancies in ZnO nanosheets enhance CO_2 electrochemical reduction to CO," Angew. Chem., Int. Ed. Engl. **57**, 6054–6059 (2018).
[86]D. Grenoble and M. M. Estadt, "The chemistry and catalysis of the water gas shift reaction 1. The kinetics over supported metal catalysts," J. Catal. **67**, 90–102 (1981).
[87]K. Ding, A. Gulec, and A. M. Johnson, "Identification of active sites in CO oxidation and water-gas shift over supported Pt catalysts," Science **350**, 189–192 (2015).
[88]M. Ojeda, R. Nabar, and A. U. Nilekar, "CO activation pathways and the mechanism of Fischer–Tropsch synthesis," J. Catal. **272**, 287–297 (2010).
[89]H. Schulz, "Short history and present trends of Fischer–Tropsch synthesis," Appl. Catal. A **186**, 3–12 (1999).
[90]N.-T. Suen, Z.-R. Kong, and C.-S. Hsu, "Morphology manipulation of copper nanocrystals and product selectivity in the electrocatalytic reduction of carbon dioxide," ACS Catal. **9**, 5217–5222 (2019).
[91]M. Ma, B. J. Trześniewski, J. Xie, and W. A. Smith, "Selective and efficient reduction of carbon dioxide to carbon monoxide on oxide-derived nanostructured silver electrocatalysts," Angew. Chem., Int. Ed. Engl. **55**, 9748–9752 (2016).
[92]W. Zhu, R. Michalsky, and Ö. Metin, "Monodisperse Au nanoparticles for selective electrocatalytic reduction of CO_2 to CO," J. Am. Chem. Soc. **135**, 16833–16836 (2013).
[93]A. Salehi-Khojin, H.-R. M. Jhong, and B. A. Rosen, "Nanoparticle silver catalysts that show enhanced activity for carbon dioxide electrolysis," J. Phys. Chem. C **117**, 1627–1632 (2013).
[94]X. Feng, K. Jiang, S. Fan, and M. W. Kanan, "Grain-boundary-dependent CO_2 electroreduction activity," J. Am. Chem. Soc. **137**, 4606–4609 (2015).
[95]C. Kim, T. Eom, and M. S. Jee, "Insight into electrochemical CO_2 reduction on surface-molecule-mediated Ag nanoparticles," ACS Catal. **7**, 779–785 (2016).
[96]Q. Lu, J. Rosen, and Y. Zhou, "A selective and efficient electrocatalyst for carbon dioxide reduction," Nat. Commun. **5**, 3242 (2014).
[97]S. Back, J.-H. Kim, Y.-T. Kim, and Y. Jung, "Bifunctional interface of Au and Cu for improved CO_2 electroreduction," ACS Appl. Mater. Interfaces **8**, 23022–23027 (2016).
[98]G. Yin, H. Abe, and R. Kodiyath, "Selective electro- or photo-reduction of carbon dioxide to formic acid using a Cu–Zn alloy catalyst," J. Mater. Chem. A **5**, 12113–12119 (2017).
[99]K. Kočí, K. Matějů, and L. Obalová, "Effect of silver doping on the TiO_2 for photocatalytic reduction of CO_2," Appl. Catal. B **96**, 239–244 (2010).
[100]T. Mizuno, K. Ohta, and A. Sasaki, "Effect of temperature on electrochemical reduction of high-pressure CO_2 with In, Sn, and Pb electrodes," Energy Sources **17**, 503–508 (1995).
[101]B. Hu, V. Stancovski, M. Morton, and S. L. Suib, "Enhanced electrocatalytic reduction of CO_2/H_2O to paraformaldehyde at Pt/metal oxide interfaces," Appl. Catal., A **382**, 277–283 (2010).
[102]M. Todoroki, K. Hara, A. Kudo, and T. Sakata, "Electrochemical reduction of high pressure CO_2 at Pb, Hg and In electrodes in an aqueous $KHCO_3$ solution," J. Electroanal. Chem. **394**, 199–203 (1995).
[103]J. Wu, F. G. Risalvato, F.-S. Ke, P. J. Pellechia, and X.-D. Zhou, "Electrochemical reduction of carbon dioxide I. Effects of the electrolyte on the selectivity and activity with Sn electrode," J. Electrochem. Soc. **159**, F353–F359 (2012).
[104]P. Bumroongsakulsawat and G. H. Kelsall, "Effect of solution pH on CO: formate formation rates during electrochemical reduction of aqueous CO_2 at Sn cathodes," Electrochim. Acta **141**, 216–225 (2014).
[105]Y. Hori, I. Takahashi, O. Koga, and N. Hoshi, "Selective formation of C_2 compounds from electrochemical reduction of CO_2 at a series of copper single crystal electrodes," J. Phys. Chem. B **106**, 15–17 (2002).
[106]Y. Hori, I. Takahashi, O. Koga, and N. Hoshi, "Electrochemical reduction of carbon dioxide at various series of copper single crystal electrodes," J. Mol. Catal. A: Chem. **199**, 39–47 (2003).
[107]C. W. Li and M. W. Kanan, "CO_2 reduction at low overpotential on Cu electrodes resulting from the reduction of thick Cu_2O films," J. Am. Chem. Soc. **134**, 7231–7234 (2012).

[108]Y. Wang, J. Liu, Y. Wang, A. M. Al-Enizi, and G. Zheng, "Tuning of CO_2 reduction selectivity on metal electrocatalysts," Small **13**, 1701809 (2017).
[109]M. Ma, K. Djanashvili, and W. A. Smith, "Controllable hydrocarbon formation from the electrochemical reduction of CO_2 over Cu nanowire arrays," Angew. Chem., Int. Ed. Engl. **55**, 6680–6684 (2016).
[110]R. Reske, H. Mistry, F. Behafarid, B. Roldan Cuenya, and P. Strasser, "Particle size effects in the catalytic electroreduction of CO_2 on Cu nanoparticles," J. Am. Chem. Soc. **136**, 6978–6986 (2014).
[111]E. L. Clark, C. Hahn, T. F. Jaramillo, and A. T. Bell, "Electrochemical CO_2 reduction over compressively strained CuAg surface alloys with enhanced multicarbon oxygenate selectivity," J. Am. Chem. Soc. **139**, 15848–15857 (2017).
[112]T. T. H. Hoang, S. Verma, and S. Ma, "Nanoporous copper–silver alloys by additive-controlled electrodeposition for the selective electroreduction of CO_2 to ethylene and ethanol," J. Am. Chem. Soc. **140**, 5791–5797 (2018).
[113]D. Kim, J. Resasco, Y. Yu, A. M. Asiri, and P. Yang, "Synergistic geometric and electronic effects for electrochemical reduction of carbon dioxide using gold-copper bimetallic nanoparticles," Nat. Commun. **5**, 4948 (2014).
[114]S. Ma, M. Sadakiyo, and M. Heima, "Electroreduction of carbon dioxide to hydrocarbons using bimetallic Cu–Pd catalysts with different mixing patterns," J. Am. Chem. Soc. **139**, 47–50 (2017).
[115]J. Jiao, R. Lin, S. Liu, and W.-C. Cheong, "Copper atom-pair catalyst anchored on alloy nanowires for selective and efficient electrochemical reduction of CO_2," Nat. Chem. **11**, 222–228 (2019).
[116]W. Luo, X. Nie, M. J. Janik, and A. Asthagiri, "Facet dependence of CO_2 reduction paths on Cu electrodes," ACS Catal. **6**, 219–229 (2015).
[117]Z. Wang, G. Yang, Z. Zhang, M. Jin, and Y. Yin, "Selectivity on etching: Creation of high-energy facets on copper nanocrystals for CO_2 electrochemical reduction," ACS Nano **10**, 4559–4564 (2016).
[118]Y. A. Wu, I. McNulty, and C. Liu, "Facet-dependent active sites of a single Cu_2O particle photocatalyst for CO_2 reduction to methanol," Nat. Energy **4**, 957–968 (2019).
[119]X. Feng, K. Jiang, S. Fan, and M. W. Kanan, "A direct grain-boundary-activity correlation for CO electroreduction on Cu nanoparticles," ACS Cent. Sci. **2**, 169–174 (2016).
[120]S. Back, H. Kim, and Y. Jung, "On the selective heterogeneous CO_2 electroreduction to methanol," ACS Catal. **5**, 965–971 (2015).
[121]A. J. Garza, A. T. Bell, and M. Head-Gordon, "Mechanism of CO_2 reduction at copper surfaces: Pathways to C_2 products," ACS Catal. **8**, 1490–1499 (2018).
[122]A. D. Handoko, K. W. Chan, and B. S. Yeo, "$-CH_3$ mediated pathway for the electroreduction of CO_2 to ethane and ethanol on thick oxide-derived copper catalysts at low overpotentials," ACS Energy Lett. **2**, 2103–2109 (2017).
[123]M. Jouny, W. Luc, and F. Jiao, "General techno-economic analysis of CO_2 electrolysis systems," Ind. Eng. Chem. Res. **57**, 2165–2177 (2018).
[124]L. An and R. Chen, "Direct formate fuel cells: A review," J. Power Sources **320**, 127–139 (2016).
[125]X. Yang, P. Pachfule, Y. Chen, N. Tsumori, and Q. Xu, "Highly efficient hydrogen generation from formic acid using a reduced graphene oxide-supported AuPd nanoparticle catalyst," Chem. Commun. **52**, 4171–4174 (2016).
[126]M. Pérez-Fortes, J. C. Schöneberger, A. Boulamanti, G. Harrison, and E. Tzimas, "Formic acid synthesis using CO_2 as raw material: Techno-economic and environmental evaluation and market potential," Int. J. Hydrogen Energy **41**, 16444–16462 (2016).
[127]A. S. Agarwal, Y. Zhai, D. Hill, and N. Sridhar, "The electrochemical reduction of carbon dioxide to formate/formic acid: Engineering and economic feasibility," ChemSusChem **4**, 1301–1310 (2011).
[128]X. Lu, D. Y. C. Leung, H. Wang, M. K. H. Leung, and J. Xuan, "Electrochemical reduction of carbon dioxide to formic acid," ChemElectroChem **1**, 836–849 (2014).
[129]J. S. Yoo, R. Christensen, T. Vegge, J. K. Nørskov, and F. Studt, "Theoretical insight into the trends that guide the electrochemical reduction of carbon dioxide to formic acid," ChemSusChem **9**, 358–363 (2016).
[130]Y. Liu, J. Zhao, and Q. Cai, "Pyrrolic–nitrogen doped graphene: A metal-free electrocatalyst with high efficiency and selectivity for the reduction of carbon dioxide to formic acid: A computational study," Phys. Chem. Chem. Phys. **18**, 5491–5498 (2016).
[131]H. Wang, J. Jia, and P. Song, "Efficient electrocatalytic reduction of CO_2 by nitrogen-doped nanoporous carbon/carbon nanotube membranes: A step towards the electrochemical CO_2 refinery," Angew. Chem., Int. Ed. Engl. **56**, 7847–7852 (2017).
[132]H. Wang and A. L. Rogach, "Hierarchical SnO_2 nanostructures: Recent advances in design, synthesis, and applications," Chem. Mater. **26**, 123–133 (2013).
[133]D. H. Won, C. H. Choi, J. Chung, and S. I. Woo, "Rational design of a hierarchical tin dendrite electrode for efficient electrochemical reduction of CO_2," ChemSusChem **8**, 3092–3098 (2015).
[134]Q. Zhu, J. Ma, and X. Kang, "Efficient reduction of CO_2 into formic acid on a lead or tin electrode using an ionic liquid catholyte mixture," Angew. Chem., Int. Ed. Engl. **55**, 9012–9016 (2016).
[135]W. Lv, R. Zhang, P. Gao, and L. Lei, "Studies on the faradaic efficiency for electrochemical reduction of carbon dioxide to formate on tin electrode," J. Power Sources **253**, 276–281 (2014).
[136]C. Cui, J. Han, and X. Zhu, "Promotional effect of surface hydroxyls on electrochemical reduction of CO_2 over SnO/Sn electrode," J. Catal. **343**, 257–265 (2016).
[137]S. Zhao, S. Li, and T. Guo, "Advances in Sn-based catalysts for electrochemical CO_2 reduction," Nano-Micro Lett. **11**, 62 (2019).
[138]M. Pourbaix and J. Burbank, "Atlas D-equilibres electrochimiques," J. Electrochem. Soc. **111**(1), 14C (1964).
[139]M. Jitaru, D. A. Lowy, and M. Toma, "Electrochemical reduction of carbon dioxide on flat metallic cathodes," J. Appl. Electrochem. **27**, 875–889 (1997).
[140]D. Kopljar, A. Inan, P. Vindayer, N. Wagner, and E. Klemm, "Electrochemical reduction of CO_2 to formate at high current density using gas diffusion electrodes," J. Appl. Electrochem. **44**, 1107–1116 (2014).
[141]Y. Chen and M. W. Kanan, "Tin oxide dependence of the CO_2 reduction efficiency on tin electrodes and enhanced activity for tin/tin oxide thin-film catalysts," J. Am. Chem. Soc. **134**, 1986–1989 (2012).
[142]K. Saravanan, Y. Basdogan, J. Dean, and J. A. Keith, "Computational investigation of CO_2 electroreduction on tin oxide and predictions of Ti, V, Nb and Zr dopants for improved catalysis," J. Mater. Chem. A **5**, 11756–11763 (2017).
[143]H. Hu, L. Gui, and W. Zhou, "Partially reduced Sn/SnO_2 porous hollow fiber: A highly selective, efficient and robust electrocatalyst towards carbon dioxide reduction," Electrochim. Acta **285**, 70–77 (2018).
[144]S. Liu, F. Pang, and Q. Zhang, "Stable nanoporous Sn/SnO_2 composites for efficient electroreduction of CO_2 to formate over wide potential range," Appl. Mater. Today **13**, 135–143 (2018).
[145]X. An, S. Li, and A. Yoshida, "Electrodeposition of tin-based electrocatalysts with different surface tin species distributions for electrochemical reduction of CO_2 to HCOOH," ACS Sustainable Chem. Eng. **7**, 9360–9368 (2019).
[146]R. Zhang, W. Lv, and L. Lei, "Role of the oxide layer on Sn electrode in electrochemical reduction of CO_2 to formate," Appl. Surf. Sci. **356**, 24–29 (2015).
[147]J. T. Feaster, C. Shi, and E. R. Cave, "Understanding selectivity for the electrochemical reduction of carbon dioxide to formic acid and carbon monoxide on metal electrodes," ACS Catal. **7**, 4822–4827 (2017).
[148]M. F. Baruch, J. E. Pander, J. L. White, and A. B. Bocarsly, "Mechanistic insights into the reduction of CO_2 on tin electrodes using in situ ATR-IR spectroscopy," ACS Catal. **5**, 3148–3156 (2015).
[149]J. Wu, F. G. Risalvato, S. Ma, and X.-D. Zhou, "Electrochemical reduction of carbon dioxide III. The role of oxide layer thickness on the performance of Sn electrode in a full electrochemical cell," J. Mater. Chem. A **2**, 1647–1651 (2014).
[150]A. Dutta, A. Kuzume, and V. Kaliginedi, "Probing the chemical state of tin oxide NP catalysts during CO_2 electroreduction: A complementary operando approach," Nano Energy **53**, 828–840 (2018).
[151]W. Deng, L. Zhang, and L. Li, "Crucial role of surface hydroxyls on the activity and stability in electrochemical CO_2 reduction," J. Am. Chem. Soc. **141**, 2911–2915 (2019).
[152]S. Wang, J. Wang, and H. Xin, "Insights into electrochemical CO_2 reduction on tin oxides from first-principles calculations," Green Energy Environ. **2**, 168–171 (2017).

[153]C. W. Lee, N. H. Cho, K. D. Yang, and K. T. Nam, "Reaction mechanisms of the electrochemical conversion of carbon dioxide to formic acid on tin oxide electrodes," ChemElectroChem **4**, 2130–2136 (2017).
[154]X. Zheng, P. De Luna, and F. P. García de Arquer, "Sulfur-modulated tin sites enable highly selective electrochemical reduction of CO_2 to formate," Joule **1**, 794–805 (2017).
[155]F. Li, L. Chen, and M. Xue, "Towards a better Sn: Efficient electrocatalytic reduction of CO_2 to formate by Sn/SnS_2 derived from SnS_2 nanosheets," Nano Energy **31**, 270–277 (2017).
[156]A. Del Castillo, M. Alvarez-Guerra, and J. Solla-Gullón, "Electrocatalytic reduction of CO_2 to formate using particulate Sn electrodes: Effect of metal loading and particle size," Appl. Energy **157**, 165–173 (2015).
[157]S. Zhang, P. Kang, and T. J. Meyer, "Nanostructured tin catalysts for selective electrochemical reduction of carbon dioxide to formate," J. Am. Chem. Soc. **136**, 1734–1737 (2014).
[158]J. Gu, F. Héroguel, J. Luterbacher, and X. Hu, "Densely packed, ultra small SnO nanoparticles for enhanced activity and selectivity in electrochemical CO_2 reduction," Angew. Chem., Int. Ed. Engl. **57**, 2943–2947 (2018).
[159]Q. Zhang, Y. Zhang, and J. Mao, "Electrochemical reduction of CO_2 by SnO_x nanosheets anchored on multiwalled carbon nanotubes with tunable functional groups," ChemSusChem **12**, 1443–1450 (2019).
[160]R. Zhang, W. Lv, G. Li, and L. Lei, "Electrochemical reduction of CO_2 on SnO_2/nitrogen-doped multiwalled carbon nanotubes composites in $KHCO_3$ aqueous solution," Mater. Lett. **141**, 63–66 (2015).
[161]W. Xiong, J. Yang, and L. Shuai, "CuSn alloy nanoparticles on nitrogen-doped graphene for electrocatalytic CO_2 reduction," ChemElectroChem **6**, 5951–5957 (2019).
[162]F. Lei, W. Liu, Y. Sun, and Y. Xie, "Metallic tin quantum sheets confined in graphene toward high-efficiency carbon dioxide electroreduction," Nat. Commun. **7**, 12697 (2016).
[163]A. Del Castillo, M. Alvarez-Guerra, and J. Solla-Gullón, "Sn nanoparticles on gas diffusion electrodes: Synthesis, characterization and use for continuous CO_2 electroreduction to formate," J. CO_2 Util. **18**, 222–228 (2017).
[164]H. Yang, Y. Huang, and J. Deng, "Selective electrocatalytic CO_2 reduction enabled by SnO_2 nanoclusters," J. Energy Chem. **37**, 93–96 (2019).
[165]B. Kumar, V. Atla, and J. P. Brian, "Reduced SnO_2 porous nanowires with a high density of grain boundaries as catalysts for efficient electrochemical CO_2-into-HCOOH conversion," Angew. Chem., Int. Ed. Engl. **56**, 3645–3649 (2017).
[166]L. Fan, Z. Xia, M. Xu, Y. Lu, and Z. Li, "1D SnO_2 with wire-in-tube architectures for highly selective electrochemical reduction of CO_2 to C_1 products," Adv. Funct. Mater. **28**, 1706289 (2018).
[167]H. Hu, Y. Wang, and N. Du, "Thermal-treatment-induced Cu–Sn core/shell nanowire array catalysts for highly efficient CO_2 electroreduction," ChemElectroChem **5**, 3854–3858 (2018).
[168]X. An, S. Li, and A. Yoshida, "Bi-doped SnO nanosheets supported on Cu foam for electrochemical reduction of CO_2 to HCOOH," ACS Appl. Mater. Interfaces **11**, 42114–42122 (2019).
[169]G. Liu, Z. Li, and J. Shi, "Black reduced porous SnO_2 nanosheets for CO_2 electroreduction with high formate selectivity and low overpotential," Appl. Catal., B **260**, 118134 (2020).
[170]W. Luc, C. Collins, and S. Wang, "Ag-Sn bimetallic catalyst with a core-shell structure for CO_2 reduction," J. Am. Chem. Soc. **139**, 1885–1893 (2017).
[171]X. Su, X.-F. Yang, Y. Huang, B. Liu, and T. Zhang, "Single-atom catalysis toward efficient CO_2 conversion to CO and formate products," Acc. Chem. Res. **52**, 656–664 (2019).
[172]T. Zheng, K. Jiang, and N. Ta, "Large-scale and highly selective CO_2 electrocatalytic reduction on nickel single-atom catalyst," Joule **3**, 265–278 (2019).
[173]X. Wang, Z. Chen, and X. Zhao, "Regulation of coordination number over single Co sites: Triggering the efficient electroreduction of CO_2," Angew. Chem. **130**, 1962–1966 (2018).
[174]Y. Wang, Z. Chen, and P. Han, "Single-atomic Cu with multiple oxygen vacancies on ceria for electrocatalytic CO_2 reduction to CH_4," ACS Catal. **8**, 7113–7119 (2018).
[175]C. Zhao, X. Dai, and T. Yao, "Ionic exchange of metal-organic frameworks to access single nickel sites for efficient electroreduction of CO_2," J. Am. Chem. Soc. **139**, 8078–8081 (2017).
[176]H. B. Yang, S.-F. Hung, and S. Liu, "Atomically dispersed Ni(i) as the active site for electrochemical CO_2 reduction," Nat. Energy **3**, 140–147 (2018).
[177]X. Zu, X. Li, and W. Liu, "Efficient and robust carbon dioxide electroreduction enabled by atomically dispersed $Sn^{\delta+}$ sites," Adv. Mater. **31**, 1808135 (2019).
[178]K.-S. Kim, W. J. Kim, H.-K. Lim, E. K. Lee, and H. Kim, "Tuned chemical bonding ability of Au at grain boundaries for enhanced electrochemical CO_2 reduction," ACS Catal. **6**, 4443–4448 (2016).
[179]W. T. Hong, M. Risch, and K. A. Stoerzinger, "Toward the rational design of non-precious transition metal oxides for oxygen electrocatalysis," Energy Environ. Sci. **8**, 1404–1427 (2015).
[180]I. C. Man, H.-Y. Su, and F. Calle-Vallejo, "Universality in oxygen evolution electrocatalysis on oxide surfaces," ChemCatChem **3**, 1159–1165 (2011).
[181]D. Wang, X. Zhang, Y. Shen, and Z. Wu, "Ni-doped MoS_2 nanoparticles as highly active hydrogen evolution electrocatalysts," RSC Adv. **6**, 16656–16661 (2016).
[182]J. Xu, Y. Kan, and R. Huang, "Revealing the origin of activity in nitrogen-doped nanocarbons towards electrocatalytic reduction of carbon dioxide," ChemSusChem **9**, 1085–1089 (2016).
[183]M. Asano, R. Kawamura, R. Sasakawa, N. Todoroki, and T. Wadayama, "Oxygen reduction reaction activity for strain-controlled Pt-based model alloy catalysts: Surface strains and direct electronic effects induced by alloying elements," ACS Catal. **6**, 5285–5289 (2016).
[184]J. W. Vickers, D. Alfonso, and D. R. Kauffman, "Electrochemical carbon dioxide reduction at nanostructured gold, copper, and alloy materials," Energy Technol. **5**, 775–795 (2017).
[185]G. Wang, Y. Yang, D. Han, and Y. Li, "Oxygen defective metal oxides for energy conversion and storage," Nano Today **13**, 23–39 (2017).
[186]Q. Wang, Y. Lei, D. Wang, and Y. Li, "Defect engineering in earth-abundant electrocatalysts for CO_2 and N_2 reduction," Energy Environ. Sci. **12**, 1730–1750 (2019).
[187]H. Huang, H. Jia, and Z. Liu, "Understanding of strain effects in the electrochemical reduction of CO_2: Using Pd nanostructures as an ideal platform," Angew. Chem., Int. Ed. Engl. **56**, 3594–3598 (2017).
[188]R. P. Jansonius, L. M. Reid, C. N. Virca, and C. P. Berlinguette, "Strain engineering electrocatalysts for selective CO_2 reduction," ACS Energy Lett. **4**, 980–986 (2019).
[189]X. Hu, H. Yang, and M. Guo, "Synthesis and characterization of (Cu, S) Co-doped SnO_2 for electrocatalytic reduction of CO_2 to formate at low overpotential," ChemElectroChem **5**, 1330–1335 (2018).
[190]Y. Zhang, J. Liu, and Z. Wei, "Electrochemical CO_2 reduction over nitrogen-doped SnO_2 crystal surfaces," J. Energy Chem. **33**, 22–30 (2019).
[191]Y. Wei, J. Liu, F. Cheng, and J. Chen, "Mn-doped atomic SnO_2 layers for highly efficient CO_2 electrochemical reduction," J. Mater. Chem. A **7**, 19651–19656 (2019).
[192]R. G. Egdell, J. Rebane, and T. J. Walker, "Competition between initial-and final-state effects in valence-and core-level x-ray photoemission of Sb-doped SnO_2," Phys. Rev. B **59**, 1792 (1999).
[193]K. H. L. Zhang, Y. Du, and P. V. Sushko, "Hole-induced insulator-to-metal transition in $La_{1-x}Sr_xCrO_3$ epitaxial films," Phys. Rev. B **91**, 155129 (2015).
[194]A. Zhang, Y. Liang, and H. Li, "Harmonizing the electronic structures of the adsorbate and catalysts for efficient CO_2 reduction," Nano Lett. **19**, 6547–6553 (2019).
[195]A. Zhang, R. He, and H. Li, "Nickel doping in atomically thin tin disulfide nanosheets enables highly efficient CO_2 reduction," Angew. Chem., Int. Ed. Engl. **57**, 10954–10958 (2018).
[196]W. Ju, J. Zeng, and K. Bejtka, "Sn-decorated Cu for selective electrochemical CO_2 to CO conversion: Precision architecture beyond composition design," ACS Appl. Energy Mater. **2**, 867–872 (2018).
[197]S. Sarfraz, A. T. Garcia-Esparza, A. Jedidi, L. Cavallo, and K. Takanabe, "Cu–Sn bimetallic catalyst for selective aqueous electroreduction of CO_2 to CO," ACS Catal. **6**, 2842–2851 (2016).

[198]X. Zheng, Y. Ji, and J. Tang, "Theory-guided Sn/Cu alloying for efficient CO_2 electroreduction at low overpotentials," Nat. Catal. **2**, 55–61 (2018).
[199]Y.-W. Choi, F. Scholten, I. Sinev, and B. Roldan Cuenya, "Enhanced stability and CO/formate selectivity of plasma-treated SnO_x/AgO_x catalysts during CO_2 electroreduction," J. Am. Chem. Soc. **141**, 5261–5266 (2019).
[200]A. M. Ismail, G. F. Samu, Á. Balog, E. Csapó, and C. Janáky, "Composition-dependent electrocatalytic behavior of Au–Sn bimetallic nanoparticles in carbon dioxide reduction," ACS Energy Lett. **4**, 48–53 (2018).
[201]Q. Lai, N. Yang, and G. Yuan, "Highly efficient In–Sn alloy catalysts for electrochemical reduction of CO_2 to formate," Electrochem. Commun. **83**, 24–27 (2017).
[202]W. J. Dong, C. J. Yoo, and J.-L. Lee, "Monolithic nanoporous In–Sn alloy for electrochemical reduction of carbon dioxide," ACS Appl. Mater. Interfaces **9**, 43575–43582 (2017).
[203]G. Wen, D. Lee, and B. Ren, "Orbital interactions in Bi–Sn bimetallic electrocatalysts for highly selective electrochemical CO_2 reduction toward formate production," Adv. Energy Mater. **8**, 1802427 (2018).
[204]S. Y. Choi, S. K. Jeong, H. J. Kim, I.-H. Baek, and K. T. Park, "Electrochemical reduction of carbon dioxide to formate on tin–lead alloys," ACS Sustainable Chem. Eng. **4**, 1311–1318 (2016).
[205]W. Luo, W. Xie, M. Li, J. Zhang, and A. Züttel, "3D hierarchical porous indium catalyst for highly efficient electroreduction of CO_2," J. Mater. Chem. A **7**, 4505–4515 (2019).
[206]R. Hegner, L. F. M. Rosa, and F. Harnisch, "Electrochemical CO_2 reduction to formate at indium electrodes with high efficiency and selectivity in pH neutral electrolytes," Appl. Catal., B **238**, 546–556 (2018).
[207]B. Bohlen, D. Wastl, J. Radomski, V. Sieber, and L. Vieira, "Electrochemical CO_2 reduction to formate on indium catalysts prepared by electrodeposition in deep eutectic solvents," Electrochem. Commun. **110**, 106597 (2020).
[208]D. D. Williams and R. R. Miller, "Effect of water vapor on the LiOH-CO_2 reaction: Dynamic isothermal system," Ind Eng. Chem. Fundam. **9**, 454–457 (1970).
[209]J. L. White and A. B. Bocarsly, "Enhanced carbon dioxide reduction activity on indium-based nanoparticles," J. Electrochem. Soc. **163**, H410–H416 (2016).
[210]W. Ma, S. Xie, and X. G. Zhang, "Promoting electrocatalytic CO_2 reduction to formate via sulfur-boosting water activation on indium surfaces," Nat. Commun. **10**, 892 (2019).
[211]C. Ding, A. Li, S.-M. Lu, H. Zhang, and C. Li, "In situ electrodeposited indium nanocrystals for efficient CO_2 reduction to CO with low overpotential," ACS Catal. **6**, 6438–6443 (2016).
[212]S. Chu, S. Hong, J. Masa, X. Li, and Z. Sun, "Synergistic catalysis of CuO/In_2O_3 composites for highly selective electrochemical CO_2 reduction to CO," Chem. Commun. **55**, 12380–12383 (2019).
[213]H. Xiang, S. Rasul, and B. Hou, "Copper–indium binary catalyst on a gas diffusion electrode for high-performance CO_2 electrochemical reduction with record CO production efficiency," ACS Appl. Mater. Interfaces **12**, 601–608 (2020).
[214]M. Zhu, P. Tian, and J. Li, "Structure-tunable copper–indium catalysts for highly selective CO_2 electroreduction to CO or HCOOH," ChemSusChem **12**, 3955–3959 (2019).
[215]W. Luo, W. Xie, and R. Mutschler, "Selective and stable electroreduction of CO_2 to CO at the copper/indium interface," ACS Catal. **8**, 6571–6581 (2018).
[216]Z. B. Hoffman, T. S. Gray, K. B. Moraveck, T. B. Gunnoe, and G. Zangari, "Electrochemical reduction of carbon dioxide to syngas and formate at dendritic copper–indium electrocatalysts," ACS Catal. **7**, 5381–5390 (2017).
[217]O. Martin, A. J. Martín, and C. Mondelli, "Indium oxide as a superior catalyst for methanol synthesis by CO_2 hydrogenation," Angew. Chem., Int. Ed. Engl. **55**, 6261–6265 (2016).
[218]S. Rasul, D. H. Anjum, A. Jedidi, and K. Takanabe, "A highly selective copper-indium bimetallic electrocatalyst for the electrochemical reduction of aqueous CO_2 to CO," Angew. Chem., Int. Ed. Engl. **54**, 2146–2150 (2015).
[219]J. He, K. E. Dettelbach, D. A. Salvatore, T. Li, and C. P. Berlinguette, "High-throughput synthesis of mixed-metal electrocatalysts for CO_2 reduction," Angew. Chem., Int. Ed. Engl. **56**, 6068–6072 (2017).
[220]S. M. Rossnagel, H. F. Dylla, and S. A. Cohen, "AES study of the adsorption of O_2, CO, CO_2, and H_2O on indium," J. Vac. Sci. Technol. **16**, 558–561 (1979).
[221]F. Abild-Pedersen and M. P. Andersson, "CO adsorption energies on metals with correction for high coordination adsorption sites—A density functional study," Surf. Sci. **601**, 1747–1753 (2007).
[222]K. P. Kuhl, T. Hatsukade, and E. R. Cave, "Electrocatalytic conversion of carbon dioxide to methane and methanol on transition metal surfaces," J. Am. Chem. Soc. **136**, 14107–14113 (2014).
[223]Y. Liang, Y. Li, and H. Wang, "Co_3O_4 nanocrystals on graphene as a synergistic catalyst for oxygen reduction reaction," Nat. Mater. **10**, 780–786 (2011).
[224]S. Gao, Z. Sun, and W. Liu, "Atomic layer confined vacancies for atomic-level insights into carbon dioxide electroreduction," Nat. Commun. **8**, 14503 (2017).
[225]Z. Zhang, F. Ahmad, and W. Zhao, "Enhanced electrocatalytic reduction of CO_2 via chemical coupling between indium oxide and reduced graphene oxide," Nano Lett. **19**, 4029–4034 (2019).
[226]J. Ye, C. Liu, and Q. Ge, "DFT study of CO_2 adsorption and hydrogenation on the In_2O_3 surface," J. Phys. Chem. C **116**, 7817–7825 (2012).
[227]K. Sun, Z. Fan, and J. Ye, "Hydrogenation of CO_2 to methanol over In_2O_3 catalyst," J. CO_2 Util. **12**, 1–6 (2015).
[228]N. Rui, Z. Wang, and K. Sun, "CO_2 hydrogenation to methanol over Pd/In_2O_3: Effects of Pd and oxygen vacancy," Appl. Catal., B **218**, 488–497 (2017).
[229]J. Y. Y. Loh and N. P. Kherani, "In situ electronic probing of photoconductive trap states for the catalytic reduction of CO_2 by $In_2O_{3-x}OH_y$ nanorods," J. Phys. Chem. Lett. **10**, 526–532 (2019).
[230]M. Tahir and N. S. Amin, "Performance analysis of nanostructured NiO–In_2O_3/TiO_2 catalyst for CO_2 photoreduction with H_2 in a monolith photoreactor," Chem. Eng. J. **285**, 635–649 (2016).
[231]Y.-X. Pan, Y. You, and S. Xin, "Photocatalytic CO_2 reduction by carbon-coated indium-oxide nanobelts," J. Am. Chem. Soc. **139**, 4123–4129 (2017).
[232]M. Tahir, B. Tahir, N. A. Saidina Amin, and H. Alias, "Selective photocatalytic reduction of CO_2 by H_2O/H_2 to CH_4 and CH_3OH over Cu-promoted In_2O_3/TiO_2 nanocatalyst," Appl. Surf. Sci. **389**, 46–55 (2016).
[233]K. H. L. Zhang, K. Xi, M. G. Blamire, and R. G. Egdell, "P-type transparent conducting oxides," J. Phys.: Condens. Matter. **28**, 383002 (2016).
[234]P. P. Edwards, A. Porch, M. O. Jones, D. V. Morgan, and R. M. Perks, "Basic materials physics of transparent conducting oxides," Dalton Trans. **19**, 2995–3002 (2004).
[235]S. Komatsu, T. Yanagihara, Y. Hiraga, M. Tanaka, and A. Kunugi, "Electrochemical reduction of CO_2 at Sb and Bi electrodes in $KHCO_3$ solution," Denki Kagaku oyobi Kogyo Butsuri Kagaku **63**, 217–224 (1995).
[236]J. Medina-Ramos, J. L. DiMeglio, and J. Rosenthal, "Efficient reduction of CO_2 to CO with high current density using in situ or ex situ prepared Bi-based materials," J. Am. Chem. Soc. **136**, 8361–8367 (2014).
[237]P. Deng, H. Wang, and R. Qi, "Bismuth oxides with enhanced bismuth–oxygen structure for efficient electrochemical reduction of carbon dioxide to formate," ACS Catal. **10**, 743–750 (2019).
[238]S. Liu, X. F. Lu, J. Xiao, X. Wang, and X. W. D. Lou, "Bi_2O_3 nanosheets grown on multi-channel carbon matrix to catalyze efficient CO_2 electroreduction to HCOOH," Angew. Chem., Int. Ed. **58**, 13828–13833 (2019).
[239]H. Zhong, Y. Qiu, and T. Zhang, "Bismuth nanodendrites as a high performance electrocatalyst for selective conversion of CO_2 to formate," J. Mater. Chem. A **4**, 13746–13753 (2016).
[240]H. Zhang, Y. Ma, and F. Quan, "Selective electro-reduction of CO_2 to formate on nanostructured Bi from reduction of BiOCl nanosheets," Electrochem. Commun. **46**, 63–66 (2014).
[241]G. Yang, W. Miao, and Z. Yuan, "Bi quantum dots obtained via in situ photodeposition method as a new photocatalytic CO_2 reduction cocatalyst instead of noble metals: Borrowing redox conversion between Bi_2O_3 and Bi," Appl. Catal., B **237**, 302–308 (2018).
[242]J. E. Pander, M. F. Baruch, and A. B. Bocarsly, "Probing the mechanism of aqueous CO_2 reduction on post-transition-metal electrodes using ATR-IR spectroelectrochemistry," ACS Catal. **6**, 7824–7833 (2016).
[243]J. E. Pander, D. Ren, and Y. Huang, "Understanding the heterogeneous electrocatalytic reduction of carbon dioxide on oxide-derived catalysts," ChemElectroChem **5**, 219–237 (2018).

[244]W. Oh, C. K. Rhee, J. W. Han, and B. Shong, "Atomic and molecular adsorption on the Bi(111) surface: Insights into catalytic CO_2 reduction," J. Phys. Chem. C **122**, 23084–23090 (2018).
[245]M. Nolan, "Adsorption of CO_2 on heterostructures of Bi_2O_3 nanocluster-modified TiO_2 and the role of reduction in promoting CO_2 activation," ACS Omega **3**, 13117–13128 (2018).
[246]A. Walsh, D. J. Payne, R. G. Egdell, and G. W. Watson, "Stereochemistry of post-transition metal oxides: Revision of the classical lone pair model," Chem. Soc. Rev. **40**, 4455–4463 (2011).
[247]R. J. Walker, A. Pougin, and F. E. Oropeza, "Surface termination and CO_2 adsorption onto bismuth pyrochlore oxides," Chem. Mater. **28**, 90–96 (2015).
[248]J. H. Koh, D. H. Won, and T. Eom, "Facile CO_2 electro-reduction to formate via oxygen bidentate intermediate stabilized by high-index planes of Bi dendrite catalyst," ACS Catal. **7**, 5071–5077 (2017).
[249]W. Zhang, Y. Hu, and L. Ma, "Liquid-phase exfoliated ultrathin Bi nanosheets: Uncovering the origins of enhanced electrocatalytic CO_2 reduction on two-dimensional metal nanostructure," Nano Energy **53**, 808–816 (2018).
[250]P. Su, W. Xu, and Y. Qiu, "Ultrathin bismuth nanosheets as a highly efficient CO_2 reduction electrocatalyst," ChemSusChem **11**, 848–853 (2018).
[251]N. Han, Y. Wang, and H. Yang, "Ultrathin bismuth nanosheets from in situ topotactic transformation for selective electrocatalytic CO_2 reduction to formate," Nat. Commun. **9**, 1320 (2018).
[252]F. P. Garcia de Arquer, O. S. Bushuyev, and P. De Luna, "2D metal oxyhalide-derived catalysts for efficient CO_2 electroreduction," Adv. Mater. **30**, e1802858 (2018).
[253]Y. Wang, X. Zhu, and Y. Li, "Spin-orbit coupling-dominated catalytic activity of two-dimensional bismuth toward CO_2 electroreduction: Not the thinner the better," J. Phys. Chem. Lett. **10**, 4663–4667 (2019).
[254]Q. Gong, P. Ding, and M. Xu, "Structural defects on converted bismuth oxide nanotubes enable highly active electrocatalysis of carbon dioxide reduction," Nat. Commun. **10**, 2807 (2019).
[255]J. Wu, X. Li, and W. Shi, "Efficient visible-light-driven CO_2 reduction mediated by defect-engineered BiOBr atomic layers," Angew. Chem., Int. Ed. Engl. **57**, 8719–8723 (2018).
[256]L. Li, D.-K. Ma, F. Qi, W. Chen, and S. Huang, "Bi nanoparticles/Bi_2O_3 nanosheets with abundant grain boundaries for efficient electrocatalytic CO_2 reduction," Electrochim. Acta **298**, 580–586 (2019).
[257]Q. Li, Y. Zhang, and X. Zhang, "Novel Bi, BiSn, Bi_2Sn, Bi_3Sn, and Bi_4Sn catalysts for efficient electroreduction of CO_2 to formic acid," Ind. Eng. Chem. Res. **59**, 6806–6814 (2020).
[258]Z. B. Hoffman, T. S. Gray, Y. Xu, and G. Zangari, "High selectivity towards formate production by electrochemical reduction of carbon dioxide at copper–bismuth dendrites," ChemSusChem **12**, 231–239 (2019).
[259]Z. Chen, K. Mou, X. Wang, and L. Liu, "Nitrogen-doped graphene quantum dots enhance the activity of Bi_2O_3 nanosheets for electrochemical reduction of CO_2 in a wide negative potential region," Angew. Chem., Int. Ed. Engl. **57**, 12790–12794 (2018).
[260]C. H. Lee and M. W. Kanan, "Controlling H^+ vs CO_2 reduction selectivity on Pb electrodes," ACS Catal. **5**, 465–469 (2014).
[261]M. Fan, S. Garbarino, G. A. Botton, A. C. Tavares, and D. Guay, "Selective electroreduction of CO_2 to formate on 3D [100] Pb dendrites with nanometer-sized needle-like tips," J. Mater. Chem. A **5**, 20747–20756 (2017).
[262]N. Zouaoui, B. D. Ossonon, and M. Fan, "Electroreduction of CO_2 to formate on amine modified Pb electrodes," J. Mater. Chem. A **7**, 11272–11281 (2019).
[263]S. Back, J.-H. Kim, Y.-T. Kim, and Y. Jung, "On the mechanism of high product selectivity for HCOOH using Pb in CO_2 electroreduction," Phys. Chem. Chem. Phys. **18**, 9652–9657 (2016).
[264]C. X. Zhao, Y. F. Bu, W. Gao, and Q. Jiang, "CO_2 reduction mechanism on the Pb(111) surface: Effect of solvent and cations," J. Phys. Chem. C **121**, 19767–19773 (2017).
[265]C. E. Moore and E. L. Gyenge, "Tuning the composition of electrodeposited bimetallic tin-lead catalysts for enhanced activity and durability in carbon dioxide electroreduction to formate," ChemSusChem **10**, 3512–3519 (2017).
[266]J. E. Pander, J. W. J. Lum, and B. S. Yeo, "The importance of morphology on the activity of lead cathodes for the reduction of carbon dioxide to formate," J. Mater. Chem. A **7**, 4093–4101 (2019).
[267]Y. Wang, H. Hu, and Y. Sun, "Facile synthesis of nanostructural high-performance Cu–Pb electrocatalysts for CO_2 reduction," Adv. Mater. Interfaces **6**, 1801200 (2019).
[268]C. Kim, T. Möller, J. Schmidt, A. Thomas, and P. Strasser, "Suppression of competing reaction channels by Pb adatom decoration of catalytically active Cu surfaces during CO_2 electroreduction," ACS Catal. **9**, 1482–1488 (2018).
[269]K. P. Kepp, "A quantitative scale of oxophilicity and thiophilicity," Inorg. Chem. **55**, 9461–9470 (2016).
[270]K. H. L. Zhang, R. G. Egdell, and F. Offi, "Microscopic origin of electron accumulation in In_2O_3," Phys. Rev. Lett. **110**, 056803 (2013).
[271]F. E. Oropeza, I. J. Villar-Garcia, R. G. Palgrave, and D. J. Payne, "A solution chemistry approach to epitaxial growth and stabilisation of $Bi_2Ti_2O_7$ films," J. Mater. Chem. A **2**, 18241–18245 (2014).
[272]G. Fu, X. Wen, and S. Xi, "Tuning the electronic structure of NiO via Li doping for the fast oxygen evolution reaction," Chem. Mater. **31**, 419–428 (2018).
[273]Z. Shen, Y. Zhuang, and W. Li, "Increased activity in the oxygen evolution reaction by Fe^{4+}-induced hole states in perovskite $La_{1-x}Sr_xFeO_3$," J. Mater. Chem. A **8**, 4407–4415 (2020).
[274]C. Long, X. Li, and J. Guo, "Electrochemical reduction of CO_2 over heterogeneous catalysts in aqueous solution: Recent progress and perspectives," Small Methods **3**, 1800369 (2018).
[275]C. Liang, B. Kim, and S. Yang, "High efficiency electrochemical reduction of CO_2 beyond the two-electron transfer pathway on grain boundary rich ultra-small SnO_2 nanoparticles," J. Mater. Chem. A **6**, 10313–10319 (2018).
[276]K. Bejtka, J. Zeng, and A. Sacco, "Chainlike mesoporous SnO_2 as a well-performing catalyst for electrochemical CO_2 reduction," ACS Appl. Energy Mater. **2**, 3081–3091 (2019).
[277]N. Han, Y. Wang, and J. Deng, "Self-templated synthesis of hierarchical mesoporous SnO_2 nanosheets for selective CO_2 reduction," J. Mater. Chem. A **7**, 1267–1272 (2019).
[278]C. I. Shaughnessy, D. T. Jantz, and K. C. Leonard, "Selective electrochemical CO_2 reduction to CO using in situ reduced In_2O_3 nanocatalysts," J. Mater. Chem. A **5**, 22743–22749 (2017).
[279]J. Zhang, R. Yin, Q. Shao, T. Zhu, and X. Huang, "Oxygen vacancies in amorphous InO_x nanoribbons enhance CO_2 adsorption and activation for CO_2 electroreduction," Angew. Chem., Int. Ed. Engl. **58**, 5609–5613 (2019).
[280]T. Li, H. Wei, and T. Liu, "Achieving efficient CO_2 electrochemical reduction on tunable $In(OH)_3$-Coupled Cu_2O-derived hybrid catalysts," ACS Appl. Mater. Interfaces **11**, 22346–22351 (2019).
[281]Y. J. Jang, J. Lee, J. H. Kim, B. J. Lee, and J. S. Lee, "One-dimensional CuIn alloy nanowires as a robust and efficient electrocatalyst for selective CO_2-to-CO conversion," J. Power Sources **378**, 412–417 (2018).
[282]Y. Zhang, F. Li, and X. Zhang, "Electrochemical reduction of CO_2 on defect-rich Bi derived from Bi_2S_3 with enhanced formate selectivity," J. Mater. Chem. A **6**, 4714–4720 (2018).
[283]Y. Qiu, J. Du, C. Dai, W. Dong, and C. Tao, "Bismuth nano-flowers as a highly selective catalyst for electrochemical reduction of CO_2 to formate," J. Electrochem. Soc. **165**, H594–H600 (2018).
[284]S. Kim, W. J. Dong, and S. Gim, "Shape-controlled bismuth nanoflakes as highly selective catalysts for electrochemical carbon dioxide reduction to formate," Nano Energy **39**, 44–52 (2017).
[285]S. He, F. Ni, and Y. Ji, "The p-orbital delocalization of main-group metals to boost CO_2 electroreduction," Angew. Chem., Int. Ed. Engl. **57**, 16114–16119 (2018).
[286]C. Dai, Y. Qiu, and Y. He, "Controlled synthesis of a Bi_2O_3–CuO catalyst for selective electrochemical reduction of CO_2 to formate," New J. Chem. **43**, 3493–3499 (2019).
[287]D. W. Davies, A. Walsh, and J. J. Mudd, "Identification of lone pair surface states on indium oxide," J. Phys. Chem. C **123**, 1700–1709 (2019).
[288]J. Y. Zhang, W. W. Li, and R. L. Z. Hoye, "Electronic and transport properties of Li-doped NiO epitaxial thin films," J. Mater. Chem. C **6**, 2275–2282 (2018).